Journal of Computational Physics 228 (2009) 4665–4701

Contents lists available at ScienceDirect

Journal of Computational Physics

journal homepage: www.elsevier.com/locate/jcp

# The *G-Scheme*: A framework for multi-scale adaptive model reduction

M. Valorani [a,*], S. Paolucci [a,b]

[a] *Dipartimento di Meccanica e Aeronautica, University of Rome "La Sapienza", Rome, RM 00184, Italy*
[b] *Aerospace & Mechanical Engineering, University of Notre Dame, Notre Dame, IN 46556, USA*

ARTICLE INFO

*Article history:*
Received 30 July 2008
Received in revised form 13 February 2009
Accepted 9 March 2009
Available online 20 March 2009

*MSC:*
37Lxx
37Mxx
80A30
80A32
76V05

*PACS:*
02.30.Hq
02.30.Jr
02.60.–x
02.70.2c
47.70.Fw
82.40.–g

*Keywords:*
Stiff problems
Model reduction
Multiple time scales
Singular perturbation analysis

ABSTRACT

The numerical solution of mathematical models for reaction systems in general, and reacting flows in particular, is a challenging task because of the simultaneous contribution of a wide range of time scales to the system dynamics. However, the dynamics can develop very-slow and very-fast time scales separated by a range of active time scales. An opportunity to reduce the complexity of the problem arises when the fast/active and slow/active time scales gaps becomes large. We propose a numerical technique consisting of an algorithmic framework, named the *G-Scheme*, to achieve multi-scale adaptive model reduction along-with the integration of the **d**ifferential **e**quations (DEs). The method is directly applicable to initial-value ODEs and (by using the method of lines) PDEs. We assume that the dynamics is decomposed into active, slow, fast, and when applicable, invariant subspaces. The *G-Scheme* introduces locally a curvilinear frame of reference, defined by a set of orthonormal basis vectors with corresponding coordinates, attached to this decomposition. The evolution of the curvilinear coordinates associated with the active subspace is described by non-stiff DEs, whereas that associated with the slow and fast subspaces is accounted for by applying algebraic corrections derived from asymptotics of the original problem. Adjusting the active DEs dynamically during the time integration is the most significant feature of the *G-Scheme*, since the numerical integration is accomplished by solving a number of DEs typically much smaller than the dimension of the original problem, with corresponding saving in computational work. To demonstrate the effectiveness of the *G-Scheme*, we present results from illustrative as well as from relevant problems.



## 1. Introduction

Multi is probably the keyword that best identifies the current trend in numerical modeling. The next frontier in numerical simulation involves multi-physics, multi-scale, multi-disciplinary problems, possibly aimed at design or control applications. Disciplines eager of computing power range from genetics, earth climate, biology, energy and combustion, and micro/nano-science and technology, among the most prominent. This demand cannot be simply accommodated by the otherwise tremendous progress achieved in hard and soft computer power; i.e., in parallel computing and code language development.

* Corresponding author. Tel.: +39 0644585278; fax: +39 06483729.
*E-mail addresses:* mauro.valorani@uniromal.it (M. Valorani), paolucci@nd.edu (S. Paolucci).

0021-9991/$ - see front matter © 2009 Elsevier Inc. All rights reserved.
doi:10.1016/j.jcp.2009.03.011

Breakthroughs are also necessary in physical/mathematical modeling and numerical/algorithmic developments. The present work is a contribution in this direction. While we believe that the applicability of our resulting algorithm is far ranging, within the following presentation we focus primarily on chemical kinetics applications.

No longer than 10 years ago, a **d**irect **n**umerical **s**imulation (DNS) [1] of a turbulent flame with a four-step kinetics mechanism on a 10 mm box constituted the state-of-the-art in combustion simulation. Nowadays, the targets are DNSs of turbulent combustion of surrogate fuels, in half-a-meter domains. The numerical integration of the mathematical model of reactive flows involving detailed hydrocarbon kinetics with hundreds of species and thousands of reactions is a formidable task because of the wide range of time scales, which can easily span 10 orders of magnitude, characterizing these large kinetic mechanisms.

The interaction of transport processes with reactions generates both thin spatial layers and temporal stiffness. Standard remedies to face these challenges are the use of adaptive mesh refinements or wavelet adaptive multilevel representations [2] to deal with thin spatial structures, and (semi-)implicit time advancement of the numerical integration. However, these approaches can be successfully pursued only when the number of unknowns in the problem is not very large.

One way to reduce the size of the problem, i.e., the number of unknowns, is to resort to model reduction techniques, such as QSSA [3,4], CSP [5,6], or ILDM [7], combined with storage-retrieval [8,9] techniques, where the reduction is obtained by prescribing a (small) number of parameters which are used to construct a look-up-table from which all required information can be reconstructed. The strength of these tools relies on a corpus of theoretical results obtained by exploiting asymptotic properties of dissipative dynamical systems, which ensures that, under proper conditions, the actual dimension of the dissipative system might be much smaller than the original size. This lower dimensional subspace, the **s**low **i**nvariant **m**anifold (SIM), can be tabulated by means of a small number of free parameters. With the reduced dimension, this approach allows in principle to eliminate the stiffness, since by construction the reduced model is freed from the action of the fast scales. However, look-up-tables suffer the curse of dimensionality, which makes problems with dimension larger than typically 20 intractable. This constraint essentially prevents the effective use of any of these techniques with detailed reaction mechanisms of hydrocarbons. Lastly, these methods do not deal at all with the presence of initial transients, thus a stiff system has to be integrated until such time that the solution comes sufficiently close to the SIM.

A promising route is offered by the successive application of different tools, each aimed at obtaining a model of dimension smaller than that of the model upon which the tool is applied. Thus, the original detailed kinetics mechanism (say of 500 species) can be simplified by removing redundant species and reactions (DRG [10], DRGEP [11], CSP [12], Time-life analysis [13]) and its dimension reduced accordingly (say to 100 species). Then, species with similar thermo-chemical and kinetics properties, typically isomers, can be lumped [14] into new generalized species, so as to obtain a further dimensional reduction (say to 70 species). Finally, QSSA is applied to bring the surviving number of species to about 20, so that ILDM-like and storage-retrieval techniques can be effectively applied. Clearly, the whole process is not only cumbersome, but at each stage one adds more and more approximations/inaccuracies, whose ultimate impact on the accuracy of the reactive flow simulation is difficult to detect, trace, and estimate. Basically, this strategy is a brilliant, but time consuming, engineering approach to deal with problems otherwise intractable to date.

The present work deals with model reduction concepts that are used to develop a time accurate computational tool that is able to exploit, adaptively, opportunities for reduction from both fast/active and slow/active spectral gaps. The class of multiscale problems which can be efficiently addressed with the new framework is that of stiff problems characterized by fast dissipative time scales, whereas, in its present form, the algorithm can achieve little or no reduction for problems characterized by slow/fast oscillations. Operationally, the new framework is designed to deal with the same class of problems as those handled efficiently by BDF methods.

The proposed numerical technique consists of an algorithmic framework, that for convenience will be referred to as the *G-Scheme*, to achieve model reduction along-with the numerical integration of a set of **d**ifferential **e**quations (DEs). The method is directly applicable to initial-value **o**rdinary **d**ifferential **e**quations (ODEs), and by using the method of lines to **p**artial **d**ifferential **e**quations (PDEs) as well. We describe the *G-Scheme* as a "framework", since, as will become apparent, the scheme is a modular procedure, where several of its components can be replaced or improved, while the overall framework remains unchanged, and can be used in different ways to achieve different goals.

The rationale used in constructing the *G-Scheme* is as follows. The construction of reduced models for a dynamical system whose asymptotic behavior might involve fixed equilibrium points, or nontrivial limit sets, such as limit cycles or chaotic attractors, is strictly related to the occurrence of a gap in the spectrum of its characteristic time scales (time-scale separation). A temporal gap separates fast modes relaxing towards a SIM from the slow modes that drive the system, whereas for systems possessing nontrivial invariant limit sets, the temporal dichotomy is between stable and unstable modes. In both cases, the most relevant asymptotic behavior of the system is confined to an invariant set which is attracting: the SIM or the limit attractor.

The characterization of the local structure of these invariant subspaces can be of great importance in the development of methods aimed at achieving a low-dimensional description of dynamical systems. The basic idea is that the invariant subspaces, ordered in a decreasing way with respect to their characteristic time scales, provide the most convenient and natural basis for describing the unstable/slow and stable/fast components of the dynamics. Consequently, model reduction can be achieved by filtering out the dynamically irrelevant degrees of freedom associated with the most stable (fast) components characterized by the most negative characteristic time scales.

Ideally, one would like to decompose the tangent space $\mathscr{T}_x$ at any point $\mathbf{x} \in \mathbb{R}^N$ into $N$ invariant subspaces, so that the dynamics within each invariant subspace is fully decoupled from all other invariant subspaces, and associated with a single characteristic time scale. This goal might easily be accomplished in linear problems, since the eigenvectors identify invariant directions, and the magnitude of eigenvalues the reciprocal of the corresponding characteristic time scales. On the other hand, the invariant geometric structure of nonlinear dynamical systems possessing nontrivial invariant sets is described by Oseledec's theorem [15]. The structure of the invariant subspaces can be formulated by introducing the concept of invariant Lyapunov–Oseledec filtrations at each point of the invariant set and the spectrum of the Lyapunov exponents. However, Oseledec's theorem does not offer a constructive method for the Lyapunov–Oseledec filtrations. The actual construction of the invariant filtrations, or even of some approximations of them [16], is, when feasible, a very time consuming task, and thus not suited to form the basis of an efficient model reduction technique.

However, the very idea of decomposing the tangent space into subspaces, not necessarily invariant, characterized by time scales of comparable magnitude is at the core of the *G-Scheme*. We assume that the tangent space $\mathscr{T}_x$ can be decomposed as the direct sum of four subspaces, $\mathscr{T}_x = \mathbb{E} \oplus \mathbb{H} \oplus \mathbb{A} \oplus \mathbb{T}$, where the active subspace $\mathbb{A}$ contains all the intermediate, or active, time scales present at that instant, all scales slower/faster than the active ones are confined in the subspaces $\mathbb{H}$ and $\mathbb{T}$, respectively, and, if the system possesses invariants, $\mathbb{E}$ is the subspace spanned by them. Using a terminology introduced in the Computational Singular Perturbation (CSP) method [17–19] in an ODE problem, $\mathbb{H}$ involves all dormant modes, $\mathbb{T}$ all fast exhausted modes, $\mathbb{A}$ all active modes, and $\mathbb{E}$ all conserved modes. In a **p**artial **d**ifferential **e**quation (PDE) problem, $\mathbb{H}$ will involve all nearly-frozen processes, $\mathbb{T}$ all near-equilibrium processes, $\mathbb{A}$ all processes in non-equilibrium, and, when applicable, $\mathbb{E}$ will involve invariants.

At each state point $\mathbf{x}$ corresponding to time $t$, the *G-Scheme* introduces a curvilinear frame of reference, defined by a set of orthonormal basis vectors with corresponding coordinates, attached to the decomposition of the tangent space in the four subspaces. At any time instant of the system evolution, the curvilinear coordinates are suitable (linear) combinations of the perturbations $\Delta\mathbf{x}$ of the original state vector $\mathbf{x}$ about $\mathbf{x}$ itself, which are assumed to be valid only within a time scale suitably defined. Thus, they can be thought of as "lumped" variables dynamically adjusting to the system's evolution.

The evolution of the curvilinear coordinates associated with the subspace $\mathbb{A}$, is described by $N_A = \dim(\mathbb{A})$ $(\leqslant N)$ differential equations, whereas the variation of the curvilinear coordinates associated with the subspaces $\mathbb{H}$ and $\mathbb{T}$ are accounted for by applying algebraic corrections derived from asymptotics of the original ODEs. Adjusting the number of active ODEs dynamically during the time integration is the most significant feature of the *G-Scheme*, because the numerical integration of the state vector $\mathbf{x} \in \mathbb{R}^N$ is obtained by solving a number of ODEs typically much smaller than $N$, with corresponding computational savings. The active ODEs evolving in $\mathbb{A}$ are freed from fast scales, and thus are non-stiff; they can be solved by resorting to any explicit scheme of integration (e.g. ERK4). When compared to a standard **b**ackward **d**ifference **f**ormula (BDF) implicit scheme used for stiff problems, the *G-Scheme* offers the advantage of requiring the solution of $N_A$ explicit ODEs instead of $N$ implicit ODEs, and the disadvantage of requiring the identification of the set of orthonormal basis vectors that defines the curvilinear frame of reference.

Fenichel's theorem [20] inspired our asymptotic treatment of the slow system related to the concept of a SIM, presented in Section 2.5, and that of the fast system, related to the concept of the bundle of fast fibers, presented in Section 2.8. Most of the model reduction techniques mentioned above, say ILDM, are deeply rooted on the possibility of exploiting the existence of a SIM. However, the experience of these past years has shown that model reduction can be achieved only when the SIM possesses specific properties, such as smoothness, uniqueness, and compactness. Another challenge associated with SIMs is that the proper SIM dimension is variable in different regions of the phase space. Not too much attention has been given to the potential of achieving model reduction by exploiting the fast fibers bundle. To the authors' knowledge, we are aware of only one approach, due to Bykov et al. [21], aimed at achieving model reduction on the basis of the fast system form during the explosive stages of the system dynamics. Indeed, the concept of fast fibers might be useful during the transient approach to a SIM, as well as during a truly explosive regime. Note that any SIM-based model reduction technique requires that the initial condition of the differential problem be on a SIM before the (slow system based) reduced model can be applied.

The concepts of SIM and fast fiber are invoked in the *G-Scheme* locally, that is, differently from other approaches, for the *G-Scheme* to be applicable it is not required that a "global" SIM exists, nor that the SIM dimension be constant or prescribed in advance. Similar comments apply to the exploitation of the fast fibers. Another unique feature of the *G-Scheme* is that both archetypes of reduction, SIM and fast fibers, collaborate to define the *G-Scheme* reduction: the SIM and the fast fiber concepts are invoked to define the $\mathbb{T}$ and $\mathbb{H}$ subspaces, respectively.

This said, the formulation in the *G-Scheme* of active ODEs follows the concept of linear embedding adopted by Adrover et al. [22]. The algebraic correction accounting for the contribution of the fast scales relies on the concept of homogeneous (radical) correction introduced in the CSP method [19,23], incorporated in the time-split explicit solver based on CSP [23], and used in the CSP/tabulation technique [24] to both create and reuse the look-up table for the CSP vectors. The algebraic correction accounting for the contribution of the slow scales relies on a local linearization of the ODEs related to the slow subspace.

Clearly, the success of the *G-Scheme* relies heavily on the ability to identify a decomposition of $\mathscr{T}_x$ which ensures minimal (ideally no) coupling among slow, fast, and active time scales. We show in Section 2.4 that the problem of finding a frame of reference yielding the maximal degree of slow/fast decoupling can be approached by resorting to the CSP refinements procedure [19,25]. In this regard, it is worth recalling that it has been proved in [26,27], for singularly perturbed problems in the canonical slow and fast system forms with an explicit constant small parameter, that the CSP refinement procedure is able to

provide the asymptotic expansion of both the SIM and fast fiber bundle, as indicated by the Fenichel theorem [20]. For simplicity, we identify in this work the set of basis vectors needed by the *G-Scheme* with the right eigenvectors of the Jacobian matrix of the vector field, this yielding a leading order approximation of the CSP vectors. The limitations associated with this choice of basis vectors when the dynamics possesses a nontrivial asymptotic behavior will be pointed out with reference to the considered numerical tests.

The paper is organized as follows. The theoretical derivations of components used by the *G-Scheme* is detailed in Section 2, the *G-Scheme* itself is presented in Section 3, and an illustrative example of the scheme is reported in Section 4 with reference to a very stiff and non-normal linear model problem. The numerical validation of the *G-Scheme* with reference to: (i) the Semenov model featuring an explosive/dissipative stiff nonlinear behavior is reported in Section 5.1, (ii) the model of an isobaric **c**ontinuously-**s**tirred **t**ank **r**eactor (CSTR) at very low pressure involving $CO/H_2$ kinetics which features a complex nonlinear behavior is reported in Section 5.2, and (iii) a reaction–diffusion [28] model exhibiting a rich dynamic structure is solved in Section 5.3. In Section 6 we provide a discussion of the *G-Scheme* and draw some conclusions.

## 2. Theory

Consider the Cauchy problem defined by a set of autonomous ODEs:

$$\frac{d\mathbf{x}(t)}{dt} = \mathbf{f}(\mathbf{x}(t)), \quad \mathbf{x}(t_0) = \mathbf{x}_0 \tag{1}$$

with time $t \in (t_0, t_f] \subset \mathbb{R}$, the state vector $\mathbf{x} \in \mathbb{R}^N$, and the nonlinear vector field $\mathbf{f} : E \subset \mathbb{R}^N \to \mathbb{R}^N$. In the case of PDEs, $N$ represents the dimension of the system after spatial discretization.

The state vector $\mathbf{x}(t)$ at time $t = t_n + \tau$, with $\tau \in \Omega \equiv (0, \Delta t] \subset \mathbb{R}$, where $\Delta t = (t_{n+1} - t_n)$, can always be expressed as the sum of the state vector $\mathbf{x}(t_n)$, for $n = 0, 1, 2, \ldots$, and a perturbation vector $\Delta\mathbf{x}(\tau)$:

$$\mathbf{x}(t) = \mathbf{x}(t_n) + \Delta\mathbf{x}(\tau). \tag{2}$$

We note that $t_n$ is some fixed arbitrary time. The component-wise representation of the perturbation vector $\Delta\mathbf{x}(\tau)$ can be expressed in terms of Cartesian coordinates $\Delta\mathbf{x} = \Delta x^i \mathbf{e}_i$, where $\mathbf{e}_i$ and $\mathbf{e}^j$ are the unit vectors of the Cartesian frame of reference, as well as in terms of curvilinear coordinates $\Delta\mathbf{x} = \Delta\xi^i \mathbf{a}_i = \Delta\xi_j \mathbf{a}^j$ related to the sets of orthonormal covariant and contravariant basis vectors $\mathbf{a}_i$ and $\mathbf{a}^j$, respectively, for which the following properties hold:

$$\mathbf{a}^i \cdot \mathbf{a}_j = \delta^i_j \quad \text{and} \quad \delta^i_j \mathbf{a}_i \mathbf{a}^j = \mathbf{1}, \tag{3}$$

where $\delta^i_j$ is the Kronecker delta symbol and $\mathbf{1}$ is the unit tensor. We adopt Einstein's notation for indices $\{i, j, k\}$. All subscript or superscript of such indices, unless otherwise noted, take on values from 1 to $N$, and repeated indices, one a superscript and the other a subscript, are to be summed; the range of other indices will be made explicit at due time. The component-wise representation of the perturbation vector $\Delta\mathbf{x}$ in the curvilinear coordinates reads:

$$\Delta\mathbf{x} = \mathbf{1} \cdot \Delta\mathbf{x} = \left(\delta^i_j \mathbf{a}_i \mathbf{a}^j\right) \cdot \Delta\mathbf{x} = \mathbf{a}_i \left(\delta^i_j \mathbf{a}^j \cdot \Delta\mathbf{x}\right) = \Delta\xi^i \mathbf{a}_i, \tag{4}$$

where

$$\Delta\xi^i = \mathbf{a}^i \cdot \Delta\mathbf{x} = \mathbf{a}^i \cdot \Delta x^j \mathbf{e}_j = b^i_j \Delta x^j \tag{5}$$

and

$$b^i_j \equiv \mathbf{a}^i \cdot \mathbf{e}_j. \tag{6}$$

Similarly, it is easy to show that

$$\Delta x^j = a^j_i \Delta\xi^i, \tag{7}$$

where

$$a^j_i \equiv \mathbf{e}^j \cdot \mathbf{a}_i \tag{8}$$

and to note that

$$a^j_i b^i_j = b^i_j a^j_i = 1. \tag{9}$$

We take a curvilinear frame of reference that varies with time. If the system is autonomous, then the frame of reference depends only on the state of the system. Subsequently, we can write

$$\mathbf{x}(t) = \mathbf{x}(t_n) + \Delta\mathbf{x}(\tau) = \mathbf{x}(t_n) + \Delta x^i(\tau)\mathbf{e}_i = \mathbf{x}(t_n) + \Delta\xi^i(\tau)\mathbf{a}_i(\tau). \tag{10}$$

Expansion (10), when substituted into (1), yields the following problem for the curvilinear coordinates:

$$\frac{d\Delta\xi^k}{d\tau} = \mathbf{a}^k(\tau)\cdot\mathbf{f}(\mathbf{x}(t_n)+\Delta\xi^i(\tau)\mathbf{a}_i(\tau)) - \mathbf{a}^k(\tau)\cdot\frac{d\mathbf{a}_i(\tau)}{d\tau}\Delta\xi^i(\tau),$$
$$\Delta\xi^k(0) = 0. \tag{11}$$

If we define

$$A(\tau)\equiv[\mathbf{a}_1(\tau)\quad\cdots\quad\mathbf{a}_i(\tau)\quad\cdots\quad\mathbf{a}_N(\tau)],\quad B(\tau)\equiv\begin{bmatrix}\mathbf{a}^1(\tau)\\ \cdots\\ \mathbf{a}^j(\tau)\\ \cdots\\ \mathbf{a}^N(\tau)\end{bmatrix},\quad \Delta\boldsymbol{\xi}(\tau)\equiv\begin{bmatrix}\Delta\xi^1(\tau)\\ \cdots\\ \Delta\xi^j(\tau)\\ \cdots\\ \Delta\xi^N(\tau)\end{bmatrix}, \tag{12}$$

where

$$A(\tau)B(\tau) = B(\tau)A(\tau) = I, \tag{13}$$

$I$ being the identity matrix, we can rewrite (11) in vector form:

$$\frac{d\Delta\boldsymbol{\xi}}{d\tau} = B(\tau)\mathbf{f}(\mathbf{x}(t_n)+A(\tau)\Delta\boldsymbol{\xi}(\tau)) - B(\tau)\frac{dA(\tau)}{d\tau}\Delta\boldsymbol{\xi}(\tau),$$
$$\Delta\boldsymbol{\xi}(0) = \mathbf{0}. \tag{14}$$

### 2.1. Invariants

Suppose that the system possesses $E$ invariant quantities $\xi^c$, where $c = 1,\ldots,E$. In (10) we can isolate the contributions to $\Delta\mathbf{x}(\tau)$ lying in the invariant subspace $\mathbb{C} = \mathbb{E}$ spanned by the vectors $\{\mathbf{a}_c\}$ from those in the orthogonal complement $\mathbb{NC}$ to $\mathbb{C}$ ($\mathbb{R}^N = \mathbb{NC}\oplus\mathbb{C}$) spanned by the vectors $\{\mathbf{a}_{c'}\}$, where $c' = E+1,\ldots,N$:

$$\mathbf{x}(t) = \mathbf{x}(t_n)+\Delta\mathbf{x}(\tau) = \mathbf{x}(t_n)+A(\tau)\Delta\boldsymbol{\xi}(\tau) = \mathbf{x}(t_n)+\Delta\xi^c(\tau)\mathbf{a}_c(\tau)+\Delta\xi^{c'}(\tau)\mathbf{a}_{c'}(\tau). \tag{15}$$

Clearly, $\Delta\xi^c(\tau)\equiv 0$ for $c = 1,\ldots,E$ because $\xi^c$ is an invariant, and therefore

$$\mathbf{x}(t) = \mathbf{x}(t_n)+\Delta\mathbf{x}(\tau) = \mathbf{x}(t_n)+\Delta\xi^{c'}(\tau)\mathbf{a}_{c'}(\tau). \tag{16}$$

Note that by construction $\mathbf{a}_{c'}(\tau)\cdot\mathbf{a}^c(\tau) = 0$ because the basis $\mathbf{a}_i(\tau)$ is assumed to be orthonormal.

**Remark 1.** Constructing $\Delta\mathbf{x}(\tau)$ with contributions solely in $\mathbb{NC}$ ensures that $\mathbf{x}(t)$ will preserve all invariants for $\tau\in\Omega$.

### 2.2. Slow/fast decomposition

Assume that the state vector $\mathbf{x}(\tau)$ can be decomposed into slow and fast components:

$$\mathbf{x}(t) = \mathbf{x}(t_n)+\Delta\mathbf{x}(\tau) = \mathbf{x}(t_n)+\Delta\xi^{c'}(\tau)\mathbf{a}_{c'}(\tau) = \mathbf{x}(t_n)+\Delta\mathbf{s}(\tau)+\Delta\mathbf{r}(\tau), \tag{17}$$

where the perturbation vectors $\Delta\mathbf{s}(\tau)$ and $\Delta\mathbf{r}(\tau)$ are defined as

$$\Delta\mathbf{s}(\tau)\equiv\Delta\xi^s(\tau)\mathbf{a}_s(\tau) = A_s(\tau)\Delta\xi^s(\tau)\quad\text{and}\quad\Delta\mathbf{r}(\tau)\equiv\Delta\xi^r(\tau)\mathbf{a}_r(\tau) = A_r(\tau)\Delta\xi^r(\tau), \tag{18}$$

$s = E+1,\ldots,M, r = M+1,\ldots,N$, and $\Delta\xi^s$ and $\Delta\xi^r$ are the amplitudes of the perturbations along the slow and fast directions $\mathbf{a}_s(\tau)$ and $\mathbf{a}_r(\tau)$, respectively. From now on, we will refer to $\Delta\xi^s$ and $\Delta\xi^r$ as slow and fast coordinates, respectively. The definitions "slow" and "fast" will be made more precise later.

This decomposition induces a slow/fast partitioning of (14):

$$\frac{d}{d\tau}\begin{pmatrix}\Delta\xi^s(\tau)\\ \Delta\xi^r(\tau)\end{pmatrix} = \begin{pmatrix}B^s(\tau)\\ B^r(\tau)\end{pmatrix}\mathbf{f}(\mathbf{x}(t_n)+\Delta\mathbf{s}(\tau)+\Delta\mathbf{r}(\tau)) - \begin{pmatrix}B^s(\tau)\frac{dA_s(\tau)}{d\tau} & B^s(\tau)\frac{dA_r(\tau)}{d\tau}\\ B^r(\tau)\frac{dA_s(\tau)}{d\tau} & B^r(\tau)\frac{dA_r(\tau)}{d\tau}\end{pmatrix}\begin{pmatrix}\Delta\xi^s(\tau)\\ \Delta\xi^r(\tau)\end{pmatrix}, \tag{19}$$

$$\begin{pmatrix}\Delta\xi^s(0)\\ \Delta\xi^r(0)\end{pmatrix} = \begin{pmatrix}\mathbf{0}^s\\ \mathbf{0}^r\end{pmatrix}, \tag{20}$$

where we have introduced the decompositions

$$A(\tau) = (A_s(\tau)\ A_r(\tau)),\quad B(\tau) = \begin{pmatrix}B^s(\tau)\\ B^r(\tau)\end{pmatrix},\quad \Delta\boldsymbol{\xi}(\tau) = \begin{pmatrix}\Delta\xi^s(\tau)\\ \Delta\xi^r(\tau)\end{pmatrix} \tag{21}$$

and we see that $\Delta\xi^s$ and $\Delta\xi^r$ are obviously coupled.

**Remark 2.** The slow/fast decomposition of the tangent space is the basis of the CSP method as well as of the present work; the slow/fast decomposition in the *G-Scheme* is used to identify the slow/fast components of the *perturbation of the state*

*vector* about the reference state $\mathbf{x}(t_n)$, whereas in the CSP method it is used to identify the slow/fast components of the *vector field* at the reference state $\mathbf{x}(t_n)$.

### 2.3. Linear forms

We expand $\mathbf{f}(\mathbf{x}(t))$ about $\mathbf{x}(t_n)$, so that to leading order we have

$$\mathbf{f}(\mathbf{x}(t)) = \mathbf{f}(\mathbf{x}(t_n) + \Delta\mathbf{x}(\tau)) \approx \mathbf{f}(\mathbf{x}_n) + J(\mathbf{x}(t_n))A(\tau)\Delta\boldsymbol{\xi}(\tau), \tag{22}$$

where

$$J(\mathbf{x}(t_n)) \equiv \left[\frac{\partial \mathbf{f}}{\partial \mathbf{x}}\right]_{\mathbf{x}(t_n)} \tag{23}$$

and also note that $dA(\tau)/d\tau$ for an autonomous system is a state function since:

$$\frac{dA(\tau)}{d\tau} = \mathrm{Grad}_{\mathbf{x}} A(\tau) \cdot \frac{d\mathbf{x}(t)}{dt} = \mathrm{Grad}_{\mathbf{x}} A(\tau) \cdot \mathbf{f}(\mathbf{x}(t)). \tag{24}$$

Linearization of the vector field in (19) and (20) yields:

$$\frac{d}{d\tau}\begin{pmatrix}\Delta\xi^s(\tau)\\ \Delta\xi^r(\tau)\end{pmatrix} = \begin{pmatrix}B^s(\tau)\\ B^r(\tau)\end{pmatrix}\mathbf{f}(\mathbf{x}(t_n)) + \begin{pmatrix}\Lambda^s_s(\mathbf{x}(t_n),\tau) & \Lambda^s_r(\mathbf{x}(t_n),\tau)\\ \Lambda^r_s(\mathbf{x}(t_n),\tau) & \Lambda^r_r(\mathbf{x}(t_n),\tau)\end{pmatrix}\begin{pmatrix}\Delta\xi^s(\tau)\\ \Delta\xi^r(\tau)\end{pmatrix}, \tag{25}$$

$$\begin{pmatrix}\Delta\xi^s(0)\\ \Delta\xi^r(0)\end{pmatrix} = \begin{pmatrix}\mathbf{0}^s\\ \mathbf{0}^r\end{pmatrix}, \tag{26}$$

where now with $\{p,q\} = \{s,r\}$ we have

$$\Lambda^p_q(\mathbf{x}(t_n),\tau) \equiv B^p(\tau)\left(-\frac{dA_q(\tau)}{d\tau} + J(\mathbf{x}(t_n))A_q(\tau)\right) = \left(\frac{dB^p(\tau)}{d\tau} + B^p(\tau)J(\mathbf{x}(t_n))\right)A_q(\tau) \tag{27}$$

and we define

$$\Lambda(\mathbf{x}(t_n),\tau) \equiv \begin{pmatrix}\Lambda^s_s(\mathbf{x}(t_n),\tau) & \Lambda^s_r(\mathbf{x}(t_n),\tau)\\ \Lambda^r_s(\mathbf{x}(t_n),\tau) & \Lambda^r_r(\mathbf{x}(t_n),\tau)\end{pmatrix}. \tag{28}$$

**Remark 3.** For $\tau = 0$, the matrix $\Lambda(\mathbf{x}(t_n),\tau)$ coincides with that used in the CSP refinements.

The off-diagonal blocks $\Lambda^s_r(\mathbf{x}(t_n),\tau)$ and $\Lambda^r_s(\mathbf{x}(t_n),\tau)$ represent the "contamination" of the slow/fast dynamics due to the contributions of the fast/slow time scales. The formal solution of the linear problem (25) and (26) is given by:

$$\Delta\xi(\tau) = \left\{e^{\int_0^\tau \Lambda(\mathbf{x}(t_n),\mu)d\mu}\int_0^\tau e^{-\int_0^\theta \Lambda(\mathbf{x}(t_n),\nu)d\nu}B(\theta)d\theta\right\}\mathbf{f}(\mathbf{x}(t_n)). \tag{29}$$

If we assume that a curvilinear transformation exists so that the matrix $\Lambda(\mathbf{x}(t_n),\tau)$ is block-diagonal, i.e.

$$\Lambda^r_s(\mathbf{x}(t_n),\tau) = \Lambda^s_r(\mathbf{x}(t_n),\tau) = 0, \tag{30}$$

then (25) and (26) become

$$\frac{d}{d\tau}\begin{pmatrix}\Delta\xi^s(\tau)\\ \Delta\xi^r(\tau)\end{pmatrix} = \begin{pmatrix}B^s(\tau)\\ B^r(\tau)\end{pmatrix}\mathbf{f}(\mathbf{x}(t_n)) + \begin{pmatrix}\Lambda^s_s(\mathbf{x}(t_n),\tau) & 0\\ 0 & \Lambda^r_r(\mathbf{x}(t_n),\tau)\end{pmatrix}\begin{pmatrix}\Delta\xi^s(\tau)\\ \Delta\xi^r(\tau)\end{pmatrix}, \tag{31}$$

$$\begin{pmatrix}\Delta\xi^s(0)\\ \Delta\xi^r(0)\end{pmatrix} = \begin{pmatrix}\mathbf{0}^s\\ \mathbf{0}^r\end{pmatrix} \tag{32}$$

and (29) becomes

$$\Delta\xi^p(\tau) = \left\{e^{\int_0^\tau \Lambda^p_p(\mathbf{x}(t_n),\mu)d\mu}\int_0^\tau e^{-\int_0^\theta \Lambda^p_p(\mathbf{x}(t_n),\nu)d\nu}B^p(\theta)d\theta\right\}\mathbf{f}(\mathbf{x}(t_n)). \tag{33}$$

In addition, if we neglect the rotation of the basis vectors, i.e., $B^p(\tau) \approx B^p(0)$ and $\Lambda^p_p(\mathbf{x}(t_n),\tau) \approx \Lambda^p_p(\mathbf{x}(t_n),0)$, then

$$\Delta\xi^p(\tau) = B^p(0)\left(\frac{e^{\Lambda^p_p(\mathbf{x}(t_n),0)\tau} - I}{\Lambda^p_p(\mathbf{x}(t_n),0)}\right)\mathbf{f}(\mathbf{x}(t_n)), \tag{34}$$

$$\approx \tau B^p(0)\left[I + \frac{1}{2}\Lambda^p_p(\mathbf{x}(t_n),0)\tau + O\left(\Lambda^p_p(\mathbf{x}(t_n),0)^2\tau^2\right)\right]\mathbf{f}(\mathbf{x}(t_n)). \tag{35}$$

In (33)–(35), the dummy index $p$ can take the value of either $r$ or $s$.

### 2.4. Basis vectors and time scales

The most important decision to be taken in the implementation of the *G-Scheme* framework is the choice of a curvilinear frame of reference, i.e., a matrix $A$, yielding a maximal degree of slow/fast decoupling. In fact, the basis vectors $\mathbf{a}_i$ used to define the matrix $A$ might be found, in principle, by different means, providing that they can block-diagonalize $\Lambda(\mathbf{x}(t_n),\tau)$ in a cost efficient way.

This challenge could be approached by resorting to the CSP refinements procedure [19,25], given that the definition of the matrix $\Lambda(\mathbf{x}(t_n),\tau)$ is the same as that introduced in the standard CSP formulation. In this work, we identify the set of basis vectors $\mathbf{a}_i$ with the right eigenvectors of the Jacobian matrix $J$ of the vector field, with the dual vectors $\mathbf{a}^j$ coinciding with the left eigenvectors of $J$. This yields a leading order approximation of the CSP vectors [25]. As an estimate of the characteristic time scales, we consider the magnitude of the reciprocal of the eigenvalues of $J$, $\lambda_j$. The ordering of the basis vectors is critical for proper decomposition. Here, we order the modes according to the magnitude of the corresponding complex eigenvalues, with

$$0=\lambda_1=\cdots=\lambda_E<|\lambda_{E+1}|\leqslant\cdots\leqslant|\lambda_{H-1}|\ll|\lambda_H|\leqslant\cdots\leqslant|\lambda_T|\ll|\lambda_{T+1}|\leqslant\cdots\leqslant|\lambda_N|,$$

where

$$\begin{aligned}
&0=\lambda_1=\cdots=\lambda_E \quad \text{identify the time scales in the subspace } \mathbb{E},\\
&|\lambda_{E+1}|\leqslant\cdots\leqslant|\lambda_{H-1}| \quad \text{identify the time scales in the subspace } \mathbb{H},\\
&|\lambda_H|\leqslant\cdots\leqslant|\lambda_T| \quad \text{identify the time scales in the subspace } \mathbb{A},\\
&|\lambda_{T+1}|\leqslant\cdots\leqslant|\lambda_N| \quad \text{identify the time scales in the subspace } \mathbb{T}.
\end{aligned} \tag{36}$$

The decomposition induced by the above time scales ordering assumes that the tangent space $\mathscr{T}_x$ is given by the direct sum of four subspaces:

$$\mathscr{T}_x=\mathbb{E}\oplus\mathbb{H}\oplus\mathbb{A}\oplus\mathbb{T}, \tag{37}$$

where the active subspace $\mathbb{A}$ contains all the intermediate, currently active (dynamic) time scales, all scales slower/faster than the active ones are confined in the subspaces $\mathbb{H}/\mathbb{T}$, and, if the system possesses $E$ invariants, $\mathbb{E}$ is the subspace spanned by the directions associated with them. Moreover, $N_E=\dim(\mathbb{E})=E, N_H=\dim(\mathbb{H})=H-E-1, N_A=\dim(\mathbb{A})=T-H+1$, and $N_T=\dim(\mathbb{T})=N-T$. Note that, because of this ordering (possibly complex) eigenvalues with both negative and positive real parts can be found in $\mathbb{H}$ and $\mathbb{A}$, whereas we expect the eigenvalues in $\mathbb{T}$ to have a dominant negative real part. Indeed, this is the distinguishing feature of the class of problems for which the *G-Scheme* is expected to perform most effectively. The ratio

$$\epsilon_H\equiv\frac{|\lambda_{H-1}|}{|\lambda_H|}\ll 1 \tag{38}$$

is a measure of the spectral gap between the slow and active subspaces, while

$$\epsilon_T\equiv\frac{|\lambda_T|}{|\lambda_{T+1}|}\ll 1 \tag{39}$$

is a measure of the spectral gap between the active and fast subspaces. Since the *G-Scheme* approximates the contributions of the very-slow and very-fast time scales with asymptotic corrections, it is expected that the accuracy and efficiency of the scheme will be higher for larger spectral gaps.

The controlling (driving) time scale of the dynamics is the fastest of the active time scales present in $\mathbb{A}$, and will be of the order of the reciprocal of $|\lambda_T|$. Note that the fastest of the slow time scales is of the order of the reciprocal of $|\lambda_{H-1}|$. A parameter that will play an important role in the accuracy of the solution obtained by the *G-Scheme* is given by

$$\epsilon_{H-T}\equiv\frac{|\lambda_{H-1}|}{|\lambda_T|}. \tag{40}$$

In preparation of the derivation of the slow and fast reduced models described in the following sections, it is useful to recast the decomposition presented in (37) as

$$\mathscr{T}_x=\mathbb{E}\oplus\mathbb{H}\oplus\mathbb{A}\oplus\mathbb{T}=\mathbb{E}\oplus\mathbb{S}_s\oplus\mathbb{R}_s=\mathbb{E}\oplus\mathbb{S}_r\oplus\mathbb{R}_r \tag{41}$$

with the following definitions for

- the slow reduced model

$$\mathbb{S}_s=\mathbb{H}\oplus\mathbb{A} \quad \text{and} \quad \mathbb{R}_s=\mathbb{T}, \tag{42}$$

where

$$\begin{aligned}
&|\lambda_{E+1}|\leqslant\cdots\leqslant|\lambda_T| \quad \text{identify the time scales in } \mathbb{S}_s,\\
&|\lambda_{T+1}|\leqslant\cdots\leqslant|\lambda_N| \quad \text{identify the time scales in } \mathbb{R}_s
\end{aligned} \tag{43}$$

with $\dim(\mathbb{S}_s)=T-E=N_H+N_A, \dim(\mathbb{R}_s)=N-T=N_T$, and spectral gap $\epsilon_s=\epsilon_T\ll 1$;

- the fast reduced model

$$\mathbb{S}_r = \mathbb{H} \quad \text{and} \quad \mathbb{R}_r = \mathbb{A} \oplus \mathbb{T}, \tag{44}$$

where

$$\begin{aligned} &|\lambda_{E+1}| \leqslant \cdots \leqslant |\lambda_{H-1}| \quad \text{identify the time scales in } \mathbb{S}_r, \\ &|\lambda_H| \leqslant \cdots \leqslant |\lambda_N| \quad \text{identify the time scales in } \mathbb{R}_r \end{aligned} \tag{45}$$

with $\dim(\mathbb{S}_r) = H - E - 1 = N_H, \dim(\mathbb{R}_r) = N - H + 1 = N_A + N_T$, and spectral gap $\epsilon_r = \epsilon_H \ll 1$.

A higher-order approximation of the ideal basis vectors can be found by resorting to the CSP refinements, which consist of a two-step iterative procedure. Each application of the first step decreases the magnitude of the upper-right matrix block $\Lambda_r^s$ by an order $\epsilon_s/\epsilon_r$ for the slow/fast system. Each application of the second step decreases the magnitude of the lower-left matrix block $\Lambda_s^r$ by an order $\epsilon_r/\epsilon_s$ for the fast/slow system. Zagaris et al. [26,27] proved that for singularly perturbed problems in the canonical slow/fast system form, and with an explicit constant small parameter, the CSP refinement procedure is able to provide the asymptotic expansions of both the SIM and the tangent space of the fast fibers, as indicated by the Fenichel theorem [20].

As discussed in the Introduction, the ideal decomposition for nonlinear dynamical systems possessing nontrivial invariant sets (e.g. limit cycles, chaotic attractors, etc.) involves the invariant Lyapunov–Oseledec filtrations at each point of the invariant set and the spectrum of the Lyapunov exponents, whose actual construction, or even approximations of them [16], is, when feasible, a very time consuming task, and thus not suited as the basis of an efficient model reduction technique. Thus, model reduction techniques adopting a decomposition based on the local Jacobian (e.g. eigenvectors, CSP refinements, etc.) provide sub-optimal performance for this class of problems, as illustrated later in the numerical tests section.

### 2.5. Ideal slow reduced model

We assume that the tangent space $\mathscr{T}_x$ is decomposed into the invariant, $\mathbb{E}$, slow, $\mathbb{S}_s$, and fast, $\mathbb{R}_s$, subspaces:

$$\mathscr{T}_x = \mathbb{E} \oplus \mathbb{S}_s \oplus \mathbb{R}_s.$$

Consider a state point $\mathbf{x}(t) \in \mathbb{S}_s$, so that the vector field $\mathbf{f}(\mathbf{x}(t))$ has no component in the fast subspace $\mathbb{R}_s$ spanned by the matrix $A_r(\tau)$, that is

$$B^r(\tau)\mathbf{f}(\mathbf{x}(t)) = B^r(\tau)\mathbf{f}(\mathbf{x}(t_n) + A_s(\tau)\Delta\boldsymbol{\xi}^s(\tau) + A_r(\tau)\Delta\boldsymbol{\xi}^r(\tau)) = \mathbf{0}^r, \quad \forall \mathbf{x}(t) \in \mathbb{S}_s. \tag{46}$$

By virtue of (30) and (33), and if all the eigenvalues of $\Lambda_r^r(\mathbf{x}(t_n), \tau)$ have negative real parts,[1] we have

$$\Delta\boldsymbol{\xi}^r(\tau) = \mathbf{0}^r, \quad \forall \tau \in \Omega_s \tag{47}$$

with $\Omega_s = (0, \Delta t_s], \Delta t_s \approx 1/|\lambda_T|$, and $t_{n+1} = t_n + \Delta t_s$. Eq. (47) implies that a point $\mathbf{x}(t_n)$ initially lying in $\mathbb{S}_s$ (thus $\Delta\boldsymbol{\xi}^r(0) = \mathbf{0}^r$) stays on $\mathbb{S}_s$ and is mapped into a point $\mathbf{x}(t)$ which can be expressed in terms of slow coordinates only:

$$\mathbf{x}(t) = \mathbf{x}(t_n) + \Delta\mathbf{s}(\tau) = \mathbf{x}(t_n) + A_s(\tau)\Delta\boldsymbol{\xi}^s(\tau), \quad \forall \tau \in \Omega_s, \tag{48}$$

where $\Delta\boldsymbol{\xi}^s(\tau)$ is obtained by solving the set of non-stiff ODE's in (31), whose solution is given formally by (33) with $p = s$. Thus, $\mathbf{x}(t)$ will lie in $\mathbb{S}_s$ during the time interval $\Omega_s$, if: (i) a set of basis vectors exists which block-decouples the matrix $A(\mathbf{x}(t_n), \tau)$, and (ii) (46) holds.

To summarize, the ideal change of coordinates is such that in $\mathbb{S}_s$:

1. only the slow coordinates $\Delta\boldsymbol{\xi}^s(\tau)$ are non-zero;
2. the rates of change of $\Delta\boldsymbol{\xi}^s(\tau)$ occur on time scales related to $\Lambda_s^s(\mathbf{x}(t_n), \tau)$;
3. the controlling slow time scale is given by the fastest scale in $\Lambda_s^s(\mathbf{x}(t_n), \tau)$;
4. in the curvilinear frame of reference, the SIM is identified as the locus where the fast coordinates $\Delta\boldsymbol{\xi}^r(\tau)$ are zero.

**Remark 4.** The condition that the state point $\mathbf{x}(t)$ given by (48) will lie in $\mathbb{S}_s$ during the time interval $\Omega_s$ can be equivalently expressed either by (i) the state Eq. (46) expressing the fact that the vector field $\mathbf{f}(\mathbf{x}(t))$ has no component in the fast subspace $\mathbb{R}_s$, or (ii) by the condition that $\Delta\mathbf{r}(\tau)$ will remain identically zero in $\Omega_s$, as expressed by (47). This last result is essential in the construction and numerical integration of the slow reduced model.

### 2.6. Numerical integration of the slow reduced model

The numerical integration of the slow reduced model can be obtained by neglecting the linear off-diagonal terms in (19) and by requiring that the slow evolution of the state vector $\mathbf{x}(t)$ satisfy the following linear embedding for $\tau \in \Omega_s$:

[1] It is assumed that the SIM is normally hyperbolic.

$$\mathbf{x}(t) = \mathbf{x}(t_n) + A_s(\tau)\Delta\xi^s(\tau). \tag{49}$$

Subsequently, we can write

$$\Delta\xi^r(\tau) = \mathbf{0}^r, \tag{50}$$

$$\frac{dA_s(\tau)}{d\tau} = \mathrm{Grad}_{\mathbf{x}} A_s(\tau)\mathbf{f}(\mathbf{x}(t_n) + A_s(\tau)\Delta\xi^s(\tau)),$$

$$A_s(0) = A_s(\mathbf{x}(t_n)), \tag{51}$$

$$\frac{d\Delta\xi^s}{d\tau} = B^s(\tau)\mathbf{f}(\mathbf{x}(t_n) + A_s(\tau)\Delta\xi^s(\tau)) - B^s(\tau)\frac{dA_s(\tau)}{d\tau}\Delta\xi^s(\tau),$$

$$\Delta\xi^s(0) = \mathbf{0}^s. \tag{52}$$

At the end of the time increment we have

$$\mathbf{x}(t_{n+1}) = \mathbf{x}(t_n) + A_s(\Delta t_s)\Delta\xi^s(\Delta t_s). \tag{53}$$

Because of (50), and because the vector field $\mathbf{f}$ is projected onto the slow subspace in (52), the fast time scales do not contribute or "contaminate" the dynamics during the time period $\Omega_s$, and therefore (52) is not stiff.

**Remark 5.** The linear embedding concept used to define (49) is also used by Adrover at al. [22].

*2.6.1. Numerical integration of the slow dynamics*

The reduced model (50)–(53) can be solved using different levels of approximation. To leading order, one can assume that the basis vectors spanning the slow subspace in the time interval $\Omega_s$ do not change much, with their values equal to the values at $\tau = 0$, that is

$$A_s(\tau) \approx A_s(0) \quad \text{so that } B^s(\tau) \approx B^s(0), \tag{54}$$

which also implies that the rotation of the basis vectors in the time interval $\Omega_s$ is negligible:

$$\frac{dA_s(\tau)}{d\tau} \approx 0. \tag{55}$$

Subsequently (49) becomes

$$\mathbf{x}(t) = \mathbf{x}(t_n) + A_s(0)\Delta\xi^s(\tau) \tag{56}$$

and (52) and (53) become:

$$\frac{d\Delta\xi^s}{d\tau} = B^s(0)\mathbf{f}(\mathbf{x}(t_n) + A_s(0)\Delta\xi^s(\tau)),$$
$$\Delta\xi^s(0) = \mathbf{0}^s \tag{57}$$

with

$$\mathbf{x}^a(t_{n+1}) = \mathbf{x}(t_n) + A_s(0)\Delta\xi^s(\Delta t_s). \tag{58}$$

Eq. (57) is nonlinear and non-stiff. It can be solved using any explicit integration scheme of any order of accuracy. Within the time interval $\Omega_s$, an inner variable time integration step can be used to ensure a prescribed accuracy level for the solution of (57). However, due to the fact that we have: (i) neglected the rotation of the basis vectors, (ii) non-ideal slow/fast decoupling, and (iii) the presence of numerical truncation errors, the state $\mathbf{x}^a$ violates the SIM constraint (50), and thus $\mathbf{x}^a(t_{n+1})$ in (58) is not equal to $\mathbf{x}(t_{n+1})$ in (53). We next discuss how to enforce the SIM constraint.

*2.6.2. SIM constraint*

Enforcing the SIM constraint during the time interval $\tau \in \Omega_s$ means that (50) or, what is the same, (46) should hold in that interval. Linearizing the vector field in (46) with respect to the state vector $\mathbf{x}^\star(t_{n+1}) = \mathbf{x}(t_n) + A_s(\tau)\Delta\xi^s(\tau)$, yields

$$B^r(\mathbf{x}^\star)\mathbf{f}(\mathbf{x}^\star) + B^r(\mathbf{x}^\star)J(\mathbf{x}^\star)A_r(\mathbf{x}^\star)\Delta\xi^r(\mathbf{x}^\star) \approx \mathbf{0}^r, \tag{59}$$

which implies that

$$\Delta\xi^r_{\mathrm{SIM}}(\mathbf{x}^\star) = -(B^r(\mathbf{x}^\star)J(\mathbf{x}^\star)A_r(\mathbf{x}^\star))^{-1}B^r(\mathbf{x}^\star)\mathbf{f}(\mathbf{x}^\star). \tag{60}$$

If we ignore the rotation of the basis vector, then $\mathbf{x}^\star \to \mathbf{x}^a$, and the result expresses, to leading order, the change in the fast coordinates necessary to enforce the SIM constraint that is violated by $\mathbf{x}^a$ after integration of the slow dynamics. This is equivalent to a projection operation of the state $\mathbf{x}^a$ onto the SIM. Note that $B^r(\mathbf{x}^a)\mathbf{f}(\mathbf{x}^a)$ is the fast projection of the vector field at $\mathbf{x}^a$; given that its value on the SIM is zero, its norm is a measure of the distance of $\mathbf{x}^a$ from the SIM. The matrix $(B^r(\mathbf{x}^a)J(\mathbf{x}^a)A_r(\mathbf{x}^a))^{-1}$ has the dimension of time; its norm provides a measure of the magnitude of the fast time scales. The

final value at the end of the interval $\tau \in \Omega_s$ is obtained by adding the contribution of the fast correction (60) to the state $\mathbf{x}^a(t_{n+1})$ found after the integration of the slow dynamics:

$$\mathbf{x}(t_{n+1}) = \mathbf{x}^a(t_{n+1}) + A_r(\mathbf{x}^a(t_{n+1}))\Delta\xi^r_{\mathrm{SIM}}(\mathbf{x}^a(t_{n+1})). \tag{61}$$

**Remark 6.** Eq. (61) shows that the state vector $\mathbf{x}(t_{n+1})$ lies on the SIM by construction.

**Remark 7.** The additive term in (61) coincides with the ("radical") correction term introduced in the CSP method [19,23], incorporated in the time-split explicit solver based on CSP, and used in the CSP/tabulation technique [24] to both create and reuse the look-up table for the CSP vectors.

We note that (46) identifies the exact SIM by means of an equation of state of the type $h_{\mathrm{SIM}}(\mathbf{x}) = 0$ only when ideal basis vectors are available. Otherwise, say when the ideal basis vectors are approximated by eigenvectors, (46) identifies only an **a**pproximate SIM (ASIM), say by means of $h_{\mathrm{ASIM}}(\mathbf{x}) = 0$. Therefore, the state point $\mathbf{x}(t_{n+1})$ obtained by using (61) is such that $h_{\mathrm{SIM}}(\mathbf{x}(t_{n+1})) \neq 0$. We thus introduce an error,[2] $\epsilon_{\mathrm{SIM}}$, associated with the choice of basis vectors:

$$\epsilon_{\mathrm{SIM}}(\mathbf{x}) \equiv |h_{\mathrm{SIM}}(\mathbf{x}) - h_{\mathrm{ASIM}}(\mathbf{x})| \sim O(\epsilon_s^q), \tag{62}$$

where $\epsilon_s$ is a measure of the spectral gap in the slow reduced model, and $q$ is the polynomial degree which characterizes the accuracy of the ASIM with respect to the exact SIM. Therefore, $\epsilon_{\mathrm{SIM}}$ can be lowered when: (i) $q$ can be increased by providing more accurate basis vectors, say by one or more applications of the first step of the CSP refinements, and/or (ii) $\epsilon_s$, which provides a measure of the spectral gap that is a characteristic of the problem (and also, as discussed below, depends on a user-specified tolerance), is lowered. The error $\epsilon_{\mathrm{SIM}}$ is inherently due to the fact that the *G-Scheme* accounts for the contribution of the fast scales with the asymptotic correction (60), which is evaluated by assuming that the SIM is given by (46) where the $B^r$ matrix is typically not ideal. Finally, note that a choice of basis vectors that ensure an ideal decoupling is also able to zero out the structural error $\epsilon_{\mathrm{SIM}}$.

### 2.7. Slow reduced model dimension

The previous section discussed how to set up a slow reduced model which approximates the exact solution with a user-prescribed accuracy. To define the reduced model we still have to identify: (i) the slow subspace (tangent space decomposition and slow subspace dimension), and (ii) a state vector $\mathbf{x}$ on the slow subspace (on the SIM) from which to start the reduced integration, assuming that $\mathbf{x}^\star$ is an intermediate state that does not lie on it. Indeed, a consistent initial condition $\mathbf{x}$ for the slow reduced model should belong to the SIM underlying the reduced model. An estimate of the error introduced by the adoption of the slow reduced model is given by the distance $|\mathbf{x} - \mathbf{x}^\star|$. To minimize this error one can identify $\mathbf{x}$ as the projection of $\mathbf{x}^\star$ onto the SIM along the fast directions:

$$\mathbf{x} = \mathbf{x}^\star + A_r(\mathbf{x}^\star)\Delta\xi^r(\mathbf{x}^\star). \tag{63}$$

The projection can be accomplished if: (i) a proper slow/fast decomposition of $\mathbf{x}^\star$ is identified by a set of basis vectors $A(\mathbf{x}^\star)$ and $B(\mathbf{x}^\star)$, and (ii) the SIM dimension ensures that the distance $|\mathbf{x} - \mathbf{x}^\star|$ is smaller than a user-defined tolerance. More specifically, we prescribe that:

$$|x^j - x^{\star j}| = \left|\sum_{r=T+1}^{N} a_r^j(\mathbf{x}^\star)\Delta\xi^r(\mathbf{x}^\star)\right| < rtol^j|\mathbf{x}^{\star j}| + atol^j \equiv \mathcal{E}^j(\mathbf{x}^\star), \quad j = 1,\ldots,N, \tag{64}$$

where $rtol^j > 0$ and $atol^j > 0$ are user-defined (vector) parameters specifying the relative and absolute reduction thresholds with respect to the total variation of the state variable over the time interval, and these values are used to form a threshold vector $\boldsymbol{\mathcal{E}}$.

In (64), both the index $T$ and $\Delta\xi^r(\mathbf{x}^\star)$ need to be determined. Given that the projected value $\mathbf{x}$ has to lie on an $N_T$-dimensional slow subspace, i.e., $\mathbf{x}$ should satisfy (63), then $\Delta\xi^r(\mathbf{x}^\star)$ can be estimated as $\Delta\xi^r_{\mathrm{SIM}}(\mathbf{x}^\star)$ obtained from (60). Subsequently, (64) becomes

$$\left|\sum_{r=T+1}^{N} a_r^j(\mathbf{x}^\star)(B^r(\mathbf{x}^\star)J(\mathbf{x}^\star)A_r(\mathbf{x}^\star))^{-1}B^r(\mathbf{x}^\star)\mathbf{f}(\mathbf{x}^\star)\right| < \mathcal{E}^j(\mathbf{x}^\star). \tag{65}$$

A further simplification can be considered involving the replacement of the full matrix $(B^r(\mathbf{x}^\star)J(\mathbf{x}^\star)A_r(\mathbf{x}^\star))^{-1}$ with a diagonal matrix whose entries are the reciprocal of the real part of the eigenvalues of $J(\mathbf{x}^\star)$, that is

$$(B^r(\mathbf{x}^\star)J(\mathbf{x}^\star)A_r(\mathbf{x}^\star))^{-1} \approx D_\lambda(\mathbf{x}^\star) \equiv \mathrm{diag}\left[\frac{1}{\lambda_r(\mathbf{x}^\star)}\right]. \tag{66}$$

The quest of achieving the largest degree of reduction satisfying a user-prescribed tolerance amounts to searching for the smallest $T$ which satisfies the inequality (65). This search can be accomplished with the following algorithm:

[2] For simplicity, we assume that $h_{\mathrm{SIM}}(\mathbf{x})$ and $h_{\mathrm{ASIM}}(\mathbf{x})$ are graphs of functions.

$M = N + 1$;
Label[200];
$M = M - 1$;
$\Delta\mathbf{r}(\mathbf{x}^\star) = -A_r(\mathbf{x}^\star) D_{\lambda_r}(\mathbf{x}^\star) B^r(\mathbf{x}^\star)\mathbf{f}(\mathbf{x}^\star)$;
If $\max_{j=1,N}\{|\Delta r^j(\mathbf{x}^\star)| - \varepsilon^j(\mathbf{x}^\star)\} > 0, T = M + 1$; Return[$T$];
If $M > 1$, Goto[200];
If $M = 1, T = M$; Return[$T$];

where $T = T(\mathbf{x}^\star)$ and $N_T = N - T$ is the dimension of $\mathbb{R}_s$ at $\mathbf{x}^\star(t_{n+1})$. The case of complex eigenvalues requires a special treatment.[3] The actual implementation of this algorithm resorts to a bisection search which becomes more efficient than the sequential search described above when $N$ is large.

**Remark 8.** The structural error $\epsilon_{SIM}$ and the user-defined error $\boldsymbol{\varepsilon}$ need to satisfy the inequality

$$|\boldsymbol{\varepsilon}| > \epsilon_{SIM} \sim O(\epsilon_s^q) \tag{67}$$

to achieve model reduction, that is to satisfy (65) with $T < N$. To satisfy the above inequality, either *rtol* and *atol* have to be increased (and accept a lower accuracy in the model) or the quality of the basis vectors have to be improved.

**Remark 9.** The inequality (65) enables the identification of the dimension $N_T$ on the basis of a tolerance requirement. However, $N_T$ might be prescribed by specifying that time scales smaller than a prescribed threshold $\tau_{\min}$ should not be considered in the slow dynamics, or that $T$ not be larger than a prescribed threshold $T_{\max}$. The solution thus found will have a variable accuracy but will describe only time scales above the enforced time-scale threshold $\tau_{\min}$. The use of the *G-Scheme* in such manner provides the opportunity to generate a static reduced model.

While the ordering or the time scales is established on the basis of the (absolute) magnitudes of the (possibly complex) eigenvalues, the decision regarding the dimension of the fast subspace is carried out on the basis of the fast mode amplitudes. An explosive mode with a non-vanishing amplitude will drive out of equilibrium all modes (both dissipative and explosive) associated with time scales slower than its own. Thus, an explosive mode will always be found in the active subspace (most likely associated with the fastest active scale). On the other hand, the ordering (36) allows us to identify the slow/invariant subspaces in a very elegant way as those having the smallest/zero time scale magnitudes.

If the problem develops a number of fast scales (real negative eigenvalues) separated from the active scales by a large spectral gap, then the amplitudes of these fast modes will eventually vanish on a time scale of the order of $\tau_T$. At this epoch, the *G-Scheme* recognizes this circumstance and exploits it to reduce the number of equations to solve. As noted above, the emergence of an explosive mode with a time scale within this fast subspace will immediately force a reduction of the fast subspace dimension and a commensurate increase of the active subspace dimension.

### 2.8. Ideal fast reduced model

We assume that the tangent space $\mathscr{T}_x$ can be decomposed into the invariant, $\mathbb{E}$, slow, $\mathbb{S}_r$, and fast $\mathbb{R}_r$, subspaces:

$$\mathscr{T}_x = \mathbb{E} \oplus \mathbb{S}_r \oplus \mathbb{R}_r.$$

Following Fenichel's theory [20], from each point $\mathbf{x}$ on $\mathbb{S}_r$, with $\dim(\mathbb{S}_r) = N_H$, emanates a fast fiber $\mathscr{F}(\mathbf{x})$, such that any initial condition $\mathbf{x}(t_n) \in \mathscr{F}(\mathbf{x})$ will relax along $\mathscr{F}(\mathbf{x})$ to $\mathbb{S}_r$, if $\mathbb{S}_r$ is normally hyperbolic in $\mathbf{x}$. Given the slow/fast system decomposition (17), it follows that the state evolution over the time interval $\Omega_r$ is given by $\mathbf{x}(t) = \mathbf{x}(t_n) + \Delta\mathbf{s}(\tau) + \Delta\mathbf{r}(\tau)$, with $\mathbf{x}(t) \in \mathscr{F}(\mathbf{x})$ for $\tau \in \Omega_r$, with $\Omega_r = (0, \Delta t_r]$, $\Delta t_r \approx 1/|\lambda_N|$, and $t_{n+1} = t_n + \Delta t_r$. In the ideal case of perfect decoupling, the matrix $A_r(\mathbf{x}(t))$ spans the tangent space $\mathscr{T}_{\mathbf{x}(t)}\mathscr{F}(\mathbf{x})$.

The evolution of the slow coordinates for $\tau \in \Omega_r$, in case of ideal slow/fast decoupling, is given by (33) with $p = s$. If we look for an estimate of the contribution of the slow dynamics along the fast fiber, we can neglect the rotation of the basis during the time interval so that from (35) we can estimate (to second-order accuracy) the evolution of the state vector along the fast fiber. Subsequently, we have

$$\mathbf{x}(\tau) \approx \mathbf{x}(t_n) + \tau A_s(0) B^s(0)\left[I + \frac{1}{2}\Lambda_s^s(\mathbf{x}(t_n), 0)\tau\right]\mathbf{f}(\mathbf{x}(t_n)) + A_r(0)\Delta\xi^r(\tau), \tag{68}$$

where $\Delta\xi^r(\tau)$ is found, in the case of complete slow/fast decoupling, by solving the set of non-stiff ODE's in (31), whose solution is given formally by (33) with $p = r$.

To summarize, the ideal change of coordinates is such that along a fast fiber:

1. the rates of change of $\Delta\xi^r(\tau)$ occur on time scales related to the matrix $\Lambda_r^r(\mathbf{x}(t_n), \tau)$;
2. the controlling fast time scale is the fastest scale in $\Lambda_r^r(\mathbf{x}(t_n), \tau)$;
3. along the fast fiber passing through the state point $\mathbf{x}(t_n)$, the contribution of the $N_H$ (slow) coordinates is approximately accounted for by (68).

[3] The contribution of a complex pair of eigenvalues needs to be formed before making the comparison with the threshold vector $\boldsymbol{\varepsilon}$.

### 2.9. Numerical integration of the fast reduced model

A numerical integration scheme of the fast reduced model can be obtained by neglecting the linear coupling terms in (19), and by requiring that the fast evolution of the state vector $\mathbf{x}(t)$ satisfies the linear embedding (17) valid for $\tau \in \Omega_r$. Thus,

$$\Delta\xi^s(\tau) = \tau B^s(0)\left[I + \frac{1}{2}\Lambda_s^s(\mathbf{x}(t_n),0)\tau\right]\mathbf{f}(\mathbf{x}(t_n)), \tag{69}$$

$$\frac{dA_s(\tau)}{d\tau} = \mathrm{Grad}_{\mathbf{x}}A_s(\tau)\mathbf{f}(\mathbf{x}(t_n) + A_s(\tau)\Delta\xi^s(\tau) + A_r(\tau)\Delta\xi^r(\tau)),$$
$$A_s(0) = A_s(\mathbf{x}(t_n)), \tag{70}$$

$$\frac{dA_r(\tau)}{d\tau} = \mathrm{Grad}_{\mathbf{x}}A_r(\tau)\mathbf{f}(\mathbf{x}(t_n) + A_s(\tau)\Delta\xi^s(\tau) + A_r(\tau)\Delta\xi^r(\tau)),$$
$$A_r(0) = A_r(\mathbf{x}(t_n)), \tag{71}$$

$$\frac{d\Delta\xi^r}{d\tau} = B^r(\tau)\mathbf{f}(\mathbf{x}(t_n) + A_s(\tau)\Delta\xi^s(\tau) + A_r(\tau)\Delta\xi^r(\tau)) - B^r(\tau)\frac{dA_r(\tau)}{d\tau}\Delta\xi^r(\tau),$$
$$\Delta\xi^r(0) = \mathbf{0}^r. \tag{72}$$

Subsequently, we have

$$\mathbf{x}(t_{n+1}) = \mathbf{x}(t_n) + A_s(\Delta t_r)\Delta\xi^s(\Delta t_r) + A_r(\Delta t_r)\Delta\xi^r(\Delta t_r). \tag{73}$$

Eq. (73) indicates that along a fast fiber, and during a time interval $\Omega_r$, the state evolution is affected by both the fast and slow time scales. To evaluate the fast time scales contribution requires the integration of (72), whereas the slow time scales contribution can be accounted for (to second-order accuracy) by the algebraic expression (69).

#### 2.9.1. Numerical integration of the fast dynamics

The reduced model (69)–(71), (73) can be solved to different levels of approximation. To leading order, one can assume that the basis vectors in the time interval $\Omega_r$ do not change much, with their value near that at $\tau = 0$, that is

$$A_i(\tau) \approx A_i(0) \quad \text{so that } B^i(\tau) \approx B^i(0), \quad \text{for } i = 1,\ldots,N, \tag{74}$$

which implies that the rotation of the basis vectors in the time interval $\Omega_r$ is negligible:

$$\frac{dA_i(\tau)}{d\tau} \approx 0 \quad \text{for } i = 1,\ldots,N. \tag{75}$$

Subsequently, (69)–(71), (73) reduce to

$$\Delta\xi^s(\tau) = \tau B^s(0)\left[I + \frac{1}{2}\Lambda_s^s(\mathbf{x}(t_n),0)\tau\right]\mathbf{f}(\mathbf{x}(t_n)), \tag{76}$$

$$\frac{d\Delta\xi^r}{d\tau} = B^r(0)\mathbf{f}(\mathbf{x}(t_n) + A_s(0)\Delta\xi^s(\tau) + A_r(0)\Delta\xi^r(\tau)),$$
$$\Delta\xi^r(0) = \mathbf{0}^r \tag{77}$$

and

$$\mathbf{x}(t_{n+1}) = \mathbf{x}(t_n) + A_s(0)\Delta\xi^s(\Delta t_r) + A_r(0)\Delta\xi^r(\Delta t_r). \tag{78}$$

Eq. (77) is nonlinear and non-stiff. It can be solved with any explicit integration scheme of any order of accuracy. Within the time interval $\Omega_r$ an inner variable time step of integration can be used to ensure a prescribed solution accuracy.

#### 2.9.2. Contribution of slow time scales

Eq. (77) implies that, even in case of perfect decoupling, the time rates of change of the fast coordinates depend on both the slow and fast contributions. This is different than in (57), where the time rate of change of the slow coordinates depends on the slow contributions only. For reasons that will become apparent, this lack of "symmetry" between the fast and slow reduced models will adversely affect the formulation of the final algorithm. Therefore, we make one additional approximation in the definition of the fast reduced model. On the time scale in which the fast modes evolve, $\tau_N = 1/|\lambda_N|$, we can neglect the slow coordinates contribution in the linear embedding for the fast system since

$$\epsilon_{H-N} \equiv \frac{|\lambda_{H-1}|}{|\lambda_N|} \ll 1. \tag{79}$$

Thus,

$$\mathbf{x}(\tau) = \mathbf{x}(t_n) + A_r(0)\Delta\xi^r(\tau) \tag{80}$$

and the following form of the fast reduced system results:

$$\begin{aligned} &\frac{d\Delta\xi^r}{d\tau} = B^r(0)\mathbf{f}(\mathbf{x}(t_n) + A_r(0)\Delta\xi^r(\tau)), \\ &\Delta\xi^r(0) = \mathbf{0}^r \end{aligned} \tag{81}$$

with

$$\mathbf{x}^a(t_{n+1}) = \mathbf{x}(t_n) + A_r(0)\Delta\xi^r(\Delta t_r). \tag{82}$$

However, since we ignored the slow coordinate contributions during the integration of (81), we apply a correction using (35) with $p = s$ to $\mathbf{x}^a(t_{n+1})$ so as to find the state $\mathbf{x}(t_{n+1})$ on the fast fiber:

$$\mathbf{x}(t_{n+1}) = \mathbf{x}^a(t_{n+1}) + A_s(0)\Delta\xi^s_{\mathrm{FF}}(\Delta t_r), \tag{83}$$

where

$$\Delta\xi^s_{\mathrm{FF}}(\Delta t_r) = \Delta t_r B^s(0)\left[I + \frac{1}{2}\Lambda^s_s(\mathbf{x}(t_n), 0)\Delta t_r\right]\mathbf{f}(\mathbf{x}(t_n)). \tag{84}$$

### 2.10. Fast reduced model dimension

We will discuss how to define the slow subspace dimension $N_H$ of $\mathbb{S}_r$ at some state $\mathbf{x}^\star$. The slow subspace $\mathbb{S}_r$ involves time scales whose contribution to the system dynamics over $\Delta t_r$, can be approximately accounted for by (84). A measure of the error can be obtained by considering the magnitude of the second-order term in (84). The criterion used to identify the slow subspace dimension $N_H$ involves finding the largest integer between $E+1$ and $N$ for which the magnitude of the second-order term is smaller than a user-defined tolerance, that is:

$$\frac{1}{2}\Delta t_r^2\left|\sum_{s=E+1}^{H-1} a^j_s(\mathbf{x}^\star)B^s(\mathbf{x}^\star)\Lambda^s_s(\mathbf{x}^\star, 0)\mathbf{f}(\mathbf{x}^\star)\right| < rtol^j|x^{\star j}| + atol^j = \varepsilon^j(\mathbf{x}^\star). \tag{85}$$

A further simplification can be safely considered which involves replacing the full matrix $\Lambda^s_s(\mathbf{x}^\star, 0)$ with a diagonal matrix whose entries are the real part of the eigenvalues of $J(\mathbf{x}^\star)$, that is

$$\Lambda^s_s(\mathbf{x}^\star, 0) \approx D_{\lambda_s}(\mathbf{x}^\star) \equiv \mathrm{diag}[\lambda_s(\mathbf{x}^\star)]. \tag{86}$$

Thus, because of (86) and since $|\lambda_s| \leqslant |\lambda_{H-1}|$ for $s = E+1, \ldots, H-1$, the inequality (85) simplifies to

$$\frac{1}{2}\Delta t_r^2\left|\sum_{s=E+1}^{H-1} \lambda_s(\mathbf{x}^\star)a^j_s(\mathbf{x}^\star)B^s(\mathbf{x}^\star)\mathbf{f}(\mathbf{x}^\star)\right| \leqslant \frac{1}{2}\epsilon_{H-N}\,\Delta t_r\left|\sum_{s=E+1}^{H-1} a^j_s(\mathbf{x}^\star)B^s(\mathbf{x}^\star)\mathbf{f}(\mathbf{x}^\star)\right| < \varepsilon^j(x^j). \tag{87}$$

The search for the largest $H$ which satisfies (87) can be accomplished with the following algorithm:

$M = E + 1$;
Label[200];
$M = M + 1$;
$\Delta\mathbf{s}_2 = 0.5\Delta t_r^2 A_s(\mathbf{x}^\star)B^s(\mathbf{x}^\star)D_{\lambda_s}(\mathbf{x}^\star)\mathbf{f}(\mathbf{x}^\star)$;
If $\max_{j=1,N}\left\{|\Delta s^j_2| - \varepsilon^j\right\} > 0, H = M - 1$; Return[$H$];
If $M < N$, Goto[200];
If $M = N, H = M$; Return[$H$];

where $N_H = H - E - 1$ is the dimension of $\mathbb{S}_r$ at state $\mathbf{x}^\star$.

## 3. The G(rappa)-Scheme

Up to this point we have discussed the formulations of the slow and fast reduced models, along-with details of the numerical approximations, by considering the separate asymptotic forms of the slow and fast dynamics of (1). However, in the most general situation, a dynamical system will develop both very-slow (dormant or near-frozen) and very-fast (or near-equilibrium) time scales. Thus, it is reasonable to look for a reduced model which can simultaneously exploit the reduction stemming from the occurrence of both very-slow and very-fast time scales. The *G-Scheme* in fact consists of an effective implementation of the merging of the slow and fast reduced models. It should be noted that the exact solution of the complete system of equations will contain all time scales inherent in the system, albeit a finite number in the case of ODEs, or a

countably-infinite number in the case of non-singular PDEs. For any arbitrary but fixed accuracy, in general there are slow and fast time scales whose dynamics are negligible and thus these modes are *not dynamically active*. Nevertheless, these near-frozen and near-equilibrium modes cannot be ignored since they play crucial roles, and thus their influence couple with those of the active modes.

### 3.1. Combined slow and fast reduced models

From Section 2.6, the slow reduced model over a time scale $\tau \in \Omega_s$ can be cast as:

$$\begin{aligned} &\Delta\xi^c \equiv \mathbf{0}^c, \quad c = 1,\dots,E, \\ &\frac{d\Delta\xi^s}{d\tau} \neq \mathbf{0}^s \quad \text{with } \Delta\xi^s(0) = \mathbf{0}^s, \quad s = E+1,\dots,T, \\ &\Delta\xi^r_{\mathrm{SIM}} \ll \mathbf{1}^r, \quad r = T+1,\dots,N \end{aligned} \tag{88}$$

and

$$\mathbf{x}(t_{n+1}) = \mathbf{x}(t_n) + A_s(\Delta t_s)\Delta\xi^s(\Delta t_s) + A_r(\Delta t_s)\Delta\xi^r_{\mathrm{SIM}}(\Delta t_s), \tag{89}$$

whereas from Section 2.9, the fast reduced model over a time scale $\tau \in \Omega_r$ can be cast as:

$$\begin{aligned} &\Delta\xi^c \equiv \mathbf{0}^c, \quad c = 1,\dots,E, \\ &\Delta\xi^s_{\mathrm{FF}} \ll \mathbf{1}^s, \quad s = E+1,\dots,H-1, \\ &\frac{d\Delta\xi^r}{d\tau} \neq \mathbf{0}^r \quad \text{with } \Delta\xi^r(0) = \mathbf{0}^r, \quad r = H,\dots,N \end{aligned} \tag{90}$$

and

$$\mathbf{x}(t_{n+1}) = \mathbf{x}(t_n) + A_r(\Delta t_r)\Delta\xi^r(\Delta t_r) + A_s(\Delta t_r)\Delta\xi^s_{\mathrm{FF}}(\Delta t_r). \tag{91}$$

Subsequently, both the slow and fast asymptotic forms can be applied to derive an appropriate reduced model of the original singularly perturbed problem. In general, the integers $T$ and $H-1$, as defined by applying the algorithms in Sections 2.7 and 2.10 that determine the dimensions of the slow and fast systems, respectively, do not coincide. This implies that a range of intermediate time scales associated with indices between $H$ and $T$ are too slow/fast to be included in the fast/slow systems, that is, their contribution to the system dynamics cannot be accounted for by asymptotics. The time scales between $H$ and $T$ (edges included) will be referred to as *active* time scales that are characteristics of all processes in the active subspace $\mathbb{A} = \mathbb{S}_s \bigcap \mathbb{R}_r$. With this notation, we can combine (88)–(91) to obtain the set of ODEs in this subspace in terms of the curvilinear coordinates $\Delta\xi^i$, with $i = 1,\dots,N$, which is valid for a time scale $\tau \in \Omega$, with $\Omega = (0, \Delta t]$, and $\Delta t \approx 1/|\lambda_T|$:

$$\Delta\xi^c \equiv \mathbf{0}^c, \quad c = 1,\dots,E, \tag{92}$$

$$\Delta\xi^h_{\mathrm{FF}} \ll \mathbf{1}^h, \quad h = E+1,\dots,H-1, \tag{93}$$

$$\frac{d\Delta\xi^a}{d\tau} = B^a(\tau)\mathbf{f}(\mathbf{x}(t_n) + A_a(\tau)\Delta\xi^a(\tau)) \quad \text{with } \Delta\xi^a(0) = \mathbf{0}^a, \quad a = H,\dots,T, \tag{94}$$

$$\Delta\xi^t_{\mathrm{SIM}} \ll \mathbf{1}^t, \quad t = T+1,\dots,N \tag{95}$$

and

$$\mathbf{x}(t_{n+1}) = \mathbf{x}(t_n) + A_h(\Delta t)\Delta\xi^h_{\mathrm{FF}}(\Delta t) + A_a(\Delta t)\Delta\xi^a(\Delta t) + A_t(\Delta t)\Delta\xi^t_{\mathrm{SIM}}(\Delta t). \tag{96}$$

By construction, the state vector $\mathbf{x}(t_{n+1})$ found by expression (96) preserves the $E$ invariants of the problem.

Eq. (93) represents slow variations of nearly invariant quantities, thus it can be thought of as a constraint having a nature similar to that exercised by (92), albeit slowly changing in time. The processes controlling the slow dynamics have a significant effect on system variations occurring over long periods of time (e.g. slow modulations of amplitude oscillations).

Eq. (95) represents an equation of state. When the basis vectors $\mathbf{a}_t$ spanning the fast subspace do not change much in time, then (95) is used to approximate the perturbations of $(N - N_T)$ "minor" (steady state, CSP radicals, etc.) state variables as functions of the rates of perturbations of $N_A$ "major" variables to generate a "static" reduced model, in the same vein as the classic QSSA and/or PEA approximations. The processes controlling the fast dynamics have a significant effect on the long term evolution of the system, since they are responsible for the emergence of SIMs.

Finally, the set of ODEs (94) represents the non-stiff time evolution of the active ("lumped") state variables. The processes controlling the active dynamics have a significant effect on system variations occurring over the driving time scale.

**Remark 10.** The spectral distance $\epsilon_{H-T}$ (see (40)) between the fastest of the slow time scales and the active time scale shows that the contribution of the slow scales can be accurately accounted by (93) (see (84) with $s \to h$) whenever $\epsilon_{H-T} \ll 1$. Clearly this is the case when $\epsilon_H \ll 1$; however, in most cases, $\epsilon_{H-T} \ll 1$ even when $\epsilon_H < 1$.

**Remark 11.** Indices similar or identical to those introduced in the CSP method to carry out a time scale-aware sensitivity analysis, can be used with minor modifications (slow, fast, and active "G-Scheme" participation and importance indices, "G-Scheme" pointers to slow, fast, and active variables/species) to extract from the *G-Scheme*-generated solutions information useful for parameter identification and mechanism simplification. This is a subject of ongoing investigation.

With reference to (92)–(96), the *G-Scheme* thus consists of: (i) the solution of $N_A$ non-stiff ODEs (94) to obtain $\mathbf{x}^a(t_{n+1})$, constrained by the linear embedding $\mathbf{x}(t) = \mathbf{x}(t_n) + A_a(\tau)\Delta\boldsymbol{\xi}^a(\tau)$, which describes the finite rate evolution of all the active processes, and (ii) application of the asymptotic corrections, the slow correction $\Delta\boldsymbol{\xi}^h_{\mathrm{FF}}$ first, which accounts for the contribution of slow scales in the subspace $\mathbb{H}$, and the fast correction $\Delta\boldsymbol{\xi}^t_{\mathrm{SIM}}$ next, which accounts for the contribution of fast scales in the subspace $\mathbb{T}$, thus ensuring that the state variable lies on the proper SIM.

The active ODEs are non-stiff because the right-hand side of (94) is obtained by projecting the vector field onto the active subspace $\mathbb{A}$, effectively filtering out both very-fast and very-slow time scales. Moreover, if we define the stiffness of the original system as $S = |\lambda_N|/|\lambda_{E+1}|$, with reference to the ordering defined in (36), then the stiffness of the active ODEs is $S_A = |\lambda_T|/|\lambda_H|$, so that $S_A \ll S$. The ratio $S/S_A$ provides an estimate of the degree of stiffness reduction.

It should be noted that both asymptotic corrections will involve a phase error directly proportional to the magnitude of the integration time step and inversely proportional to the spectral gap $\epsilon_T$ and the spectral distance $\epsilon_{H-T}$. Numerical tests confirm that the *G-Scheme* always yields an accurate solution that is consistent with the degree of reduction of active modes. As will be illustrated, the realm of application of the scheme is very large. The *G-Scheme*,[4] in effect, is a new adaptive reduction framework that we hope will enable us to tackle challenging problems without the need of preliminary analysis of any type.

### 3.2. The G-Scheme framework step-by-step

The algorithmic steps of the *G-Scheme* framework will be described in this section with reference to Fig. 1. We will use indices $i = 1,\ldots,N, a = H,\ldots,T, h = E+1,\ldots,H-1$, and $t = T+1,\ldots,N$. We wish to find a numerical solution for $t \in (t_0, t_f]$ with given initial condition $\mathbf{x}(t_0) = \mathbf{x}_0$.

We initialize the calculation by prescribing that $T(\mathbf{x}(t_0)) = N$, and compute $J(\mathbf{x}(t_0)), \lambda_i(t_0) = \lambda_i(\mathbf{x}(t_0)), A(t_0) = A(\mathbf{x}(t_0))$ and $B(t_0) = B(\mathbf{x}(t_0))$. Next, for each time interval $t_n$ ($\tau = 0$), and for the state vector $\mathbf{x}(t_n)$, with $n = 0, 1, 2, \ldots$, we proceed as follows:

1. Define the time step as:
$$\Delta t = \gamma/|\lambda_{T(\mathbf{x}(t_n))}|, \quad \gamma \leqslant 1; \tag{97}$$
2. Update time:
$$t_{n+1} = t_n + \Delta t; \tag{98}$$
3. Find $H(\mathbf{x}(t_n))$ since, as discussed in Section 2.10, it depends on $\Delta t$;
4. Solve the set of non-stiff ODE's for $\tau \in \Omega = (0, \Delta t]$:
$$\frac{d\Delta\boldsymbol{\xi}^a}{d\tau} = B^a(t_n)\mathbf{f}(\mathbf{x}(t_n) + A_a(t_n)\Delta\boldsymbol{\xi}^a(\tau)), \quad \Delta\boldsymbol{\xi}^a(0) = \mathbf{0}^a; \tag{99}$$
5. Update state vector:
$$\mathbf{x}^a(t_{n+1}) = \mathbf{x}(t_n) + A_a(t_n)\Delta\boldsymbol{\xi}^a(\Delta t); \tag{100}$$
6. Apply head correction:
$$\mathbf{x}^h(t_{n+1}) = \mathbf{x}^a(t_{n+1}) + A_h(t_n)\Delta\boldsymbol{\xi}^h_{\mathrm{FF}}(\Delta t); \tag{101}$$
where the head correction is estimated as:
$$\Delta\boldsymbol{\xi}^h_{\mathrm{FF}}(\Delta t) = \Delta t\, B^h(t_n)\left[I + \frac{1}{2}A^h_h(\mathbf{x}(t_n), t_n)\Delta t\right]\mathbf{f}(\mathbf{x}(t_n)); \tag{102}$$
7. Apply tail correction to project the solution onto the fast subspace obtained using the bases at $t_n$:
$$\mathbf{x}^t(t_{n+1}) = \mathbf{x}^h(t_{n+1}) + A_t(t_n)\Delta\boldsymbol{\xi}^t_{\mathrm{SIM}(t_n)}(\Delta t), \tag{103}$$
where the tail correction is estimated as:
$$\Delta\boldsymbol{\xi}^t_{\mathrm{SIM}(t_n)}(\Delta t) = -(B^t(t_n)J(\mathbf{x}(t_n))A_t(t_n))^{-1}B^t(t_n)\mathbf{f}(\mathbf{x}^h(t_n)); \tag{104}$$

[4] The *G* in the *G*-Scheme originates from the similarity between the action of discarding the fast and slow scales in the scheme with the distillation process followed in the production of *Grappa*, an italian liquor. The first and third fractions of the vapors distilled by fermented grapes, named *Head* and *Tail* respectively, are contaminated by poisonous alcohols and thus discarded; only the second fraction, the *Heart*, yields the *Grappa*. Thus, the active time scales are the *Heart* of the problem, *c.v.d.*

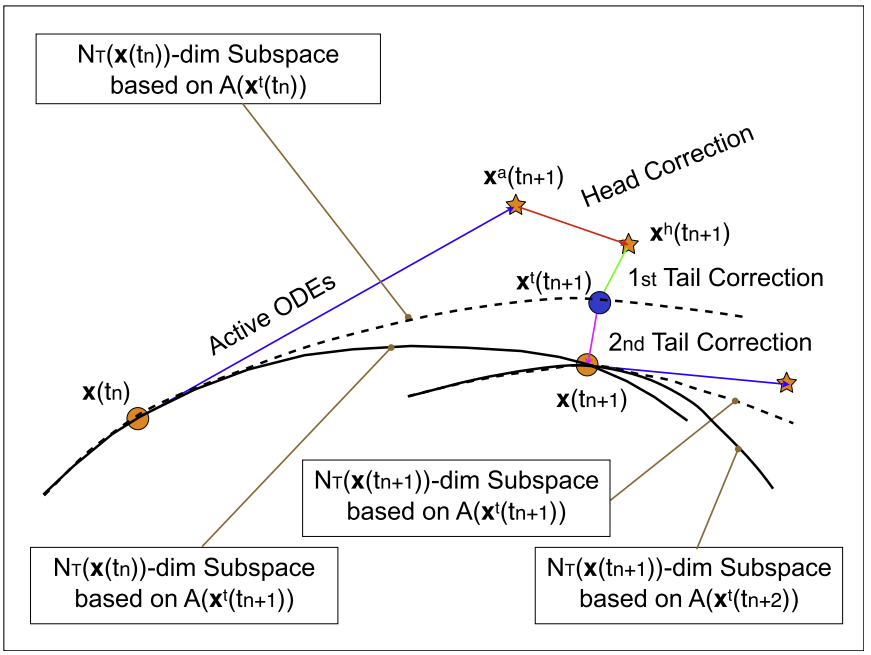


**Fig. 1.** The *G-Scheme* step-by-step starting from a given state $\mathbf{x}(t_n)$ on a subspace of dimension evaluated at $t_n$: orange stars denote intermediate new states before the application of head or tail corrections, the blue circle denotes the new state after head and tail corrections onto the subspace evaluated at $t_n$ and where the basis vectors are subsequently updated to $t_{n+1}$, orange circle denotes the new state $\mathbf{x}(t_{n+1})$ and the location where the subspace dimension possibly changes. Note that in reality the orange circles are not exactly on the SIM; we are actually calculating the ASIM. We do not show both the SIM and ASIM so as not to make the figure unduly complex. (For interpretation of the references to color in this figure legend, the reader is referred to the web version of this article.)

8. Update $J(\mathbf{x}^t(t_{n+1}))$, $\lambda_i(t_{n+1}) = \lambda_i(\mathbf{x}^t(t_{n+1}))$, and the set of new basis vectors $A(t_{n+1}) = A(\mathbf{x}^t(t_{n+1}))$ and $B(t_{n+1}) = B(\mathbf{x}^t(t_{n+1}))$;
9. Apply bases rotation correction if necessary (i.e., if the fast subspace changes) to find the state $\mathbf{x}(t_{n+1})$ by projecting $\mathbf{x}^t(t_{n+1})$ located on the manifold evaluated at $t_n$ onto the manifold evaluated at $t_{n+1}$:

$$\mathbf{x}(t_{n+1}) = \mathbf{x}^t(t_{n+1}) + A(t_{n+1})\Delta\xi_{\mathrm{SIM}(t_{n+1})}(\Delta t); \tag{105}$$

where the basis rotation correction is estimated as:

$$\Delta\xi_{\mathrm{SIM}(t_{n+1})}(\Delta t) = -(B^t(t_{n+1})J(\mathbf{x}^t(t_{n+1}))A_t(t_{n+1}))^{-1}B^t(t_{n+1})\mathbf{f}(\mathbf{x}^t(t_{n+1})); \tag{106}$$

10. Find $T(\mathbf{x}(t_{n+1}))$ as discussed in Section 2.7;
11. Update counter: $n = n + 1$;
12. If $[t_{n+1} < t_f]$ go back to step (1).

The choice of the safety factor $\gamma$ has an impact on the local error of the solution, given that $\Delta t = \gamma O(\tau_T^p)$ where $p$ is the formal order of accuracy of the quadrature scheme adopted to integrate (99).

**Remark 12.** Step (9) is essential in the *G-Scheme* as it accounts for a correction that projects the new solution, $\mathbf{x}^t(t_{n+1})$, from a fast subspace obtained using the old bases to the one obtained with the new bases. Thus, from now on, when we say that we apply a tail correction, the basis rotation correction, if necessary, is included with it; i.e., it is considered to be part-and-parcel of the tail correction.

**Remark 13.** From the above presentation it is apparent that the numerical solution generated by the *G-Scheme* approximates the trajectory of the original system by patching together trajectories obtained with reduced order models, each lying on the corresponding SIM. All the trajectories describing the transients between different SIMs in the original system (together with the associated fast scales) are not represented by the *G-Scheme*-generated solution, since their overall contribution to the system dynamics is accounted for by projection operations (tail corrections).

**Remark 14.** For PDEs, $N$ can be varied between time steps. Indeed this is natural if the *G-Scheme* is used as a solver within a spatially adaptive scheme.

*3.2.1. Higher-order form of the reduced model*

In (99) one can retain the linear terms accounting for the rotation of the basis vectors:

$$\frac{d\Delta\xi^a}{d\tau} = B^a(\tau)\mathbf{f}(\mathbf{x}(t_n) + A_a(\tau)\Delta\xi^a(\tau)) - B^a(\tau)\frac{dA_a(\tau)}{d\tau}\Delta\xi^a(\tau). \tag{107}$$

Eq. (107) can be solved using a predictor/corrector approach. A measure of the magnitude of the rotation of the basis vectors is provided by $|d\ln(J/|J|)/dt|$, which in turn measures the significance of nonlinearities. In addition, it is also possible to account for off-diagonal (coupling or "contamination") terms within a linear approximation.

*3.2.2. Higher-order estimate of the basis vectors*

As noted earlier, the basis vectors used in the reduced model can be found by resorting to the CSP vectors. Their leading order approximation is obtained by considering the eigenvectors of the Jacobian matrix of the vector field. Higher-order approximations can be found by applying one or more CSP refinements. It is conjectured that in most circumstances the higher accuracy in the identification of the basis vectors, which, by itself, is such to provide a cleaner decoupling between the slow and fast subspaces, will not translate in an increased efficiency of the scheme to an extent which will compensate for the additional work inherent with the application of the CSP refinements. Instead, one promising option, as indicated in step (9), is to compute the local basis vectors as perturbations of the previously computed basis vectors, again by resorting to a simplified version of the CSP refinements.

## 4. Illustration of the *G-Scheme* for a planar ODE model

In this section, we illustrate the main steps of the *G-Scheme* as it applies to a test model featuring a stiff and non-normal linear behavior, described by the following two-dimensional system:

$$\begin{aligned}
\epsilon\frac{dy}{dt} &= \csc(\theta-\psi)(\cos(\theta)(z(\epsilon-1)\cos(\psi) + y\sin(\psi)) - y\epsilon\cos(\psi)\sin(\theta)),\\
\epsilon\frac{dz}{dt} &= \csc(\theta-\psi)((z\epsilon\cos(\theta) - y(\epsilon-1)\sin(\theta))\sin(\psi) - z\cos(\psi)\sin(\theta)),
\end{aligned} \tag{108}$$

where the state vector is defined as $\mathbf{x} = (y, z)$, the vector field $\mathbf{f}(y, z; \psi, \theta, \epsilon)$ is defined by the right-hand side of (108), and $\epsilon < 1$ is the spectral gap; by construction, the eigenvalues of the Jacobian matrix of the right-hand sides of (108) are $\lambda_1 = -1$ and $\lambda_2 = -1/\epsilon$; the corresponding right eigenvectors are $\mathbf{a}_1(\theta) = (\cos(\theta), \sin(\theta))$ and $\mathbf{a}_2(\psi) = (\cos(\psi), \sin(\psi))$. The slow and fast time scales are given respectively by $\tau_1 = 1$ and $\tau_2 = \epsilon$. The difference $|\theta - \psi|$ measures the angle between the two eigen-directions (or the non-normality of the system).

Let us introduce the Cartesian $\{\Delta x^1, \Delta x^2\}$ and curvilinear $\{\Delta\xi^1, \Delta\xi^2\}$ coordinates, slow and fast respectively, for the perturbation vector $\Delta\mathbf{x}$. Application of the transformation (5) yields:

$$\begin{aligned}
\Delta\xi^1 &= +\csc(\psi-\theta)(\Delta z\cos(\theta) - \Delta y\sin(\theta)),\\
\Delta\xi^2 &= -\csc(\psi-\theta)(\Delta z\cos(\psi) - \Delta y\sin(\psi)).
\end{aligned} \tag{109}$$

Subsequently, the fast perturbation vector is

$$\Delta\mathbf{r}(\Delta\xi^2;\theta) = \begin{pmatrix}\cos(\theta)\\ \sin(\theta)\end{pmatrix}\Delta\xi^2, \tag{110}$$

from which it is apparent that $\Delta\mathbf{r}$ is parameterized by the fast coordinate $\Delta\xi^2$, and that the slow coordinate $\Delta\xi^1$ plays no role. Furthermore, the slow perturbation vector is given by

$$\Delta\mathbf{s}(\Delta\xi^1;\psi) = \begin{pmatrix}\cos(\psi)\\ \sin(\psi)\end{pmatrix}\Delta\xi^1 \tag{111}$$

from which it is apparent that $\Delta\mathbf{s}$ is parameterized by the slow coordinate $\Delta\xi^1$, and that the fast coordinate $\Delta\xi^2$ plays no role.

### 4.1. The slow system

The slow system describes the evolution of the slow coordinate $\Delta\xi^1$ along the SIM and for $\tau \in (0, \Delta t_s]$, with $\Delta t_s \approx O(\tau_1 = 1)$, reads:

$$\begin{aligned}
&\frac{d\Delta\xi^1}{d\tau} = \csc(\psi-\theta)(y\sin(\theta) - z\cos(\theta)) - \Delta\xi^1,\\
&\Delta\xi^1(0) = 0
\end{aligned} \tag{112}$$

showing that it is decoupled from the fast coordinate $\Delta\xi^2$. Given the linearity of (108), (112) is also linear with respect to $\Delta\xi^1$; of course, this circumstance is not typical of nonlinear systems.

The linear embedding of the slow system (53), specialized for this model and for $\tau \in (0, \Delta t_s]$, reads:

$$\mathbf{x}^a(t) = \mathbf{x} + \Delta\mathbf{s}(\tau) = \begin{pmatrix} y \\ z \end{pmatrix} + \begin{pmatrix} \cos(\psi) \\ \sin(\psi) \end{pmatrix} \Delta\xi^1(\tau). \tag{113}$$

The exact solution of (112) is

$$\Delta\xi^1(\tau) = -e^{-\tau}(-1 + e^{\tau}) \csc(\psi - \theta)(z\cos(\theta) - y\sin(\theta)), \tag{114}$$

which, after replacement in the linear embedding (113), yields the solution of the slow dynamics

$$\mathbf{x}^a(t) = \begin{pmatrix} y \\ z \end{pmatrix} - e^{-\tau}(-1 + e^{\tau}) \csc(\psi - \theta)(z\cos(\theta) - y\sin(\theta)) \begin{pmatrix} \cos(\psi) \\ \sin(\psi) \end{pmatrix}. \tag{115}$$

Note that the solution of the slow dynamics (115) contains only the slow time scale $\tau_1 = 1$ and therefore is non-stiff.

### 4.2. The fast correction

The amplitude of the fast mode is a state function and reads:

$$f^2(\mathbf{x}; \psi, \theta, \epsilon) = \mathbf{a}^2(\psi) \cdot \mathbf{f}(\mathbf{x}; \psi, \theta, \epsilon) = \frac{1}{\epsilon} \csc(\psi - \theta)(z\cos(\psi) - y\sin(\psi)). \tag{116}$$

The SIM is found by enforcing (46), and in this case has an exact representation which in implicit form is given by

$$f^2(\mathbf{x}; \psi, \theta, \epsilon) = 0 = z\cos(\psi) - y\sin(\psi). \tag{117}$$

The fast correction magnitude $\Delta\xi^2_{SIM}(\mathbf{x})$ provided by (60) is a state function and, in this case, is independent of $\epsilon$:

$$\Delta\xi^2_{\mathrm{SIM}}(\mathbf{x}; \psi, \theta) = \tau_2 f^2(\mathbf{x}; \psi, \theta, \epsilon) = \csc(\psi - \theta)(z\cos(\psi) - y\sin(\psi)). \tag{118}$$

The fast correction vector provided by

$$\mathbf{a}_2 \Delta\xi^2_{\mathrm{SIM}} = \csc(\psi - \theta)(z\cos(\psi) - y\sin(\psi)) \begin{pmatrix} \cos(\theta) \\ \sin(\theta) \end{pmatrix} \tag{119}$$

is a state function independent of $\epsilon$. Adding this contribution to the solution of the slow dynamics (61) yields the complete solution of the slow system

$$\begin{aligned} \mathbf{x}(t) &= \mathbf{x}^a(t) + \mathbf{a}_2 \Delta\xi^2_{\mathrm{SIM}}, \\ &= \begin{pmatrix} y \\ z \end{pmatrix} + \csc(\psi - \theta)(z\cos(\psi) - y\sin(\psi)) \begin{pmatrix} \cos(\theta) \\ \sin(\theta) \end{pmatrix} + e^{-\tau}(1 - e^{\tau}) \csc(\psi - \theta)(z\cos(\theta) - y\sin(\theta)) \begin{pmatrix} \cos(\psi) \\ \sin(\psi) \end{pmatrix}. \end{aligned} \tag{120}$$

It is instructive to consider the trajectories obtained for $\tau \in (0, \tau_2 = \epsilon]$ with the slow reduced model (120) and the slow dynamics (without fast correction) (115), and compare them with the exact solution of (108). This is done in Fig. 2 for $\psi = \pi/7, \theta = \pi/9$, and $\epsilon = 10^{-2}$. The initial condition for the three cases is the same $\{z_0 = 3, y_0 = z_0 \cot(\psi) - \epsilon\}$ and is $\epsilon$-close to the SIM. It is apparent that the exact solution (blue) approaches the SIM (black line) at the fast rate $\tau_2 = \epsilon = 10^{-2}$. The slow reduced model (120) (red) is forced to lie on the SIM because of the fast correction; in fact, it is well known that initial conditions of a reduced model cannot be arbitrarily prescribed since they should satisfy the algebraic constraint which defines the reduced model itself.

The error of the slow reduced model can be estimated by the $L_2$-norm between the exact solution $\mathbf{x}_{ex}$ and $\mathbf{x}$:

$$\|\mathbf{x}(t) - \mathbf{x}_{ex}(t)\|_2 = e^{-t/\epsilon}\{|\cos(\theta)\csc(\theta - \psi)(z\cos(\psi) - y\sin(\psi))|^2 + |\csc(\theta - \psi)\sin(\theta)(y\sin(\psi) - z\cos(\psi))|^2\}^{1/2}. \tag{121}$$

As indicated by (121), the error decreases at the fast rate, and on the fast scale (from the right- to the left-edges of the trajectories the time elapsed is $\tau_2 = \epsilon$) has almost vanished. This indicates that the error associated with the application of the slow reduced model is mostly confined to an initial transient, having a duration of the order of the fast time scale, which is triggered any time that the fast subspace dimension undergoes a sudden increase, this implying a projection of the state vector on a SIM of lower dimension. The slow dynamics without fast correction (120) is clearly not attracted to the SIM, since its trajectory remains parallel to it, and possibly would result in the attainment of an incorrect fixed point. Indeed, this non-vanishing error is due to an incorrect choice of initial condition (not lying on the SIM) for the slow dynamics. This simple analysis demonstrates the necessity of enforcing the fast correction to define a consistent slow reduced model.

### 4.3. The fast system

The fast system describes the evolution of the slow coordinate $\Delta\xi^2$ along a fast fiber, and for $\tau \in (0, \Delta t_r]$, with $\Delta t_r \approx \tau_2 = \epsilon$, reads:

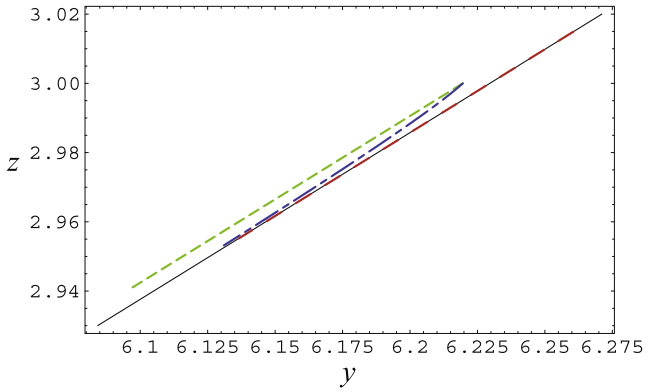


**Fig. 2.** Trajectories obtained for $\tau \in [0, \tau_2 = \epsilon], \psi = \pi/7, \theta = \pi/9, \epsilon = 10^{-2}$, and initial condition $\{z_0 = 3, y_0 = z_0 \cot(\psi) - \epsilon\}$: slow reduced model (120) (dash red line), slow dynamics (without fast correction) (115) (short-dash green line), exact solution of (108). (short-long-dash blue line), and SIM (solid black line). (For interpretation of the references to color in this figure legend, the reader is referred to the web version of this article.)

$$\begin{aligned} &\frac{\mathrm{d}\Delta\xi^2}{\mathrm{d}\tau} = \frac{1}{\epsilon}(\csc(\psi-\theta)(z\cos(\psi) - y\sin(\psi)) - \Delta\xi^2, \\ &\Delta\xi^2(0) = 0 \end{aligned} \tag{122}$$

showing that it is decoupled from the slow coordinate $\Delta\xi^1$. Given the linearity of (108), (122) is also linear with respect to $\Delta\xi^2$.

The linear embedding of the fast system (80) specialized for this model reads:

$$\mathbf{x}^a(t) = \mathbf{x} + \Delta\mathbf{r}(\tau) = \begin{pmatrix} y \\ z \end{pmatrix} + \begin{pmatrix} \cos(\theta) \\ \sin(\theta) \end{pmatrix} \Delta\xi^2(\tau). \tag{123}$$

The exact solution of (122) is

$$\Delta\xi^2(\tau) = (1 - e^{-\tau/\epsilon}) \csc(\psi-\theta)(z\cos(\psi) - y\sin(\psi)), \tag{124}$$

which, after replacement in the linear embedding, yields the solution of the fast dynamics:

$$\mathbf{x}^a(t) = \begin{pmatrix} y \\ z \end{pmatrix} + (1 - e^{-\tau/\epsilon}) \csc(\psi-\theta)(z\cos(\psi) - y\sin(\psi)) \begin{pmatrix} \cos(\theta) \\ \sin(\theta) \end{pmatrix}. \tag{125}$$

Note that this solution is not stiff since it contains only the fast time scale $\tau_2 = \epsilon$.

### 4.4. The slow correction

The evolution of the state vector along the fast fiber can be obtained as in (68) by taking the leading order term of (35). However, one can consider adding higher-order terms. In the following we will compare the accuracy of the first- and second-order approximations.

#### 4.4.1. First order

The fast fiber correction to leading order reads

$$\Delta\xi^1_{\mathrm{FF},1}(\mathbf{x}, \tau; \psi, \theta) = \tau \csc(\psi-\theta)(y\sin(\theta) - z\cos(\theta)). \tag{126}$$

The slow correction is different from the fast correction (116) in that it is not a state function but depends on $\tau$. The slow correction vector

$$\mathbf{a}_1 \Delta\xi^1_{\mathrm{FF},1}(\tau) = \tau \csc(\psi-\theta)(y\sin(\theta) - z\cos(\theta)) \begin{pmatrix} \cos(\psi) \\ \sin(\psi) \end{pmatrix} \tag{127}$$

is independent of $\epsilon$. Adding this contribution to the solution of the fast dynamics (125) yields the complete solution of the fast system, which reads

$$\begin{aligned} \mathbf{x}_1(t) &= \mathbf{x}^a(t) + \mathbf{a}_1 \Delta\xi^1_{\mathrm{FF},1}(\tau), \\ &= \begin{pmatrix} y \\ z \end{pmatrix} + \tau \csc(\psi-\theta)(y\sin\,(\theta) - z\cos(\theta)) \begin{pmatrix} \cos(\psi) \\ \sin(\psi) \end{pmatrix} + (1 - e^{-\tau/\epsilon})\ \csc(\psi-\theta)(z\cos(\psi) - y\sin(\psi)) \begin{pmatrix} \cos(\theta) \\ \sin(\theta) \end{pmatrix}. \end{aligned} \tag{128}$$

Note that this solution does depend on the spectral gap $\epsilon$. The error of the fast reduced model with a first-order accurate slow correction can be estimated by the $L_2$-norm between the exact solution $\mathbf{x}_{ex}$ and $\mathbf{x}_1$:

$$\|\mathbf{x}_1(t)-\mathbf{x}_{ex}(t)\|_2=\Big\{e^{-t}[(e^t(t-1)+1)\cos(\psi)\csc(\theta-\psi)(z\cos(\theta)-y\sin(\theta))]^2 + e^{-t}[(e^t(t-1)+1)\csc(\theta-\psi)(z\cos(\theta)-y\sin(\theta))\sin(\psi)]^2\Big\}^{1/2}. \tag{129}$$

Clearly the error grows exponentially on the slow scale, and thus this reduced model is sufficiently accurate only for times of the order of the fast scale.

*4.4.2. Second order*

The slow correction to second order reads

$$\Delta\xi^1_{\mathrm{FF},2}(\mathbf{x},\tau;\psi,\theta)=\frac{1}{2}(\tau-2)\tau\csc(\psi-\theta)(z\cos(\theta)-y\sin(\theta)). \tag{130}$$

The corresponding slow correction vector in this case is given by

$$\mathbf{a}_1\Delta\xi^1_{\mathrm{FF},2}(\tau)=\frac{1}{2}(\tau-2)\tau\csc(\psi-\theta)(z\cos(\theta)-y\sin(\theta))\begin{pmatrix}\cos(\psi)\\ \sin(\psi)\end{pmatrix}. \tag{131}$$

Adding this contribution to the solution of the fast dynamics (125) yields the complete solution of the fast system to second-order accuracy of the slow correction:

$$\begin{aligned}\mathbf{x}_2(t)&=\mathbf{x}^a(t)+\mathbf{a}_1\Delta\xi^1_{\mathrm{FF},2}(\tau),\\ &=\begin{pmatrix}y\\ z\end{pmatrix}+\frac{1}{2}(\tau-2)\tau\csc(\psi-\theta)(z\cos(\theta)-y\sin(\theta))\begin{pmatrix}\cos(\psi)\\ \sin(\psi)\end{pmatrix}+(1-e^{-\tau/\epsilon})\csc(\psi-\theta)(z\cos(\psi)-y\sin(\psi))\begin{pmatrix}\cos(\theta)\\ \sin(\theta)\end{pmatrix}.\end{aligned} \tag{132}$$

The error of the fast reduced model with a second-order accurate slow correction can be estimated by the $L_2$-norm between the exact solution $\mathbf{x}_{ex}$ and $\mathbf{x}_2$:

$$\|\mathbf{x}_2(t)-\mathbf{x}_{ex}(t)\|_2=\Big\{\frac{1}{2}e^{-t}[(e^t(t^2-2t+2)-2)\cos(\psi)\csc(\theta-\psi)(z\cos(\theta)-y\sin(\theta))]^2 + \frac{1}{2}e^{-t}[(e^t(t^2-2t+2)-2)\csc(\theta-\psi)(z\cos(\theta)-y\sin(\theta))\sin(\psi)]^2\Big\}^{1/2}. \tag{133}$$

Consider the trajectories obtained with the fast reduced models (128) and (132), and the fast dynamics (without slow correction) (125). Their comparisons with the exact solution of (108) are shown in Fig. 3. The initial condition for the three cases is the same $\{y_0=50, z_0=50\}$ and is off the SIM. The exact solution (black) evolves at the fast rate $\tau_2=\epsilon$. The fast reduced models (128) and (132) (red and blue) are close, the latter with second-order accuracy being closer to the exact solution than the former which is first-order accurate, during a time of the order of the fast scale. The fast dynamics without slow correction (125) (green) not only does not lie close to the exact solution (the error being larger for smaller spectral gaps), but the end point reaches a value much further to the right because the slow time scale has no means to slow down the purely fast dynamics.

Lastly, we note that in two-dimensional models, as long as there is one active time scale, then at any specific time only a head or tail correction to the active dynamics can be applied. A system of dimension three or larger is necessary to be able to apply both head and tail corrections at the same time.

## 5. Numerical validation

All reference solutions presented in this section are obtained with the module *NDSolve* in Mathematica© 6.0, the *Automatic* method of integration (by default an LSODA approach is used, switching between a non-stiff Adams method and a stiff Gear BDF method), a precision (or *rtol*) of $10^{-10}$, and accuracy (or *atol*) of $10^{-14}$. The calculations carried out with the *G-Scheme* use the explicit Runge–Kutta four-stage scheme (classic ERK4, (1/6;1/3;1/3;1/6)) to integrate the active dynamics, and, unless otherwise stated, we use $rtol=10^{-4}$ and $atol=10^{-13}$ in the threshold vector $\boldsymbol{\varepsilon}$ defined in (64) (and used in (65) and (87)), and $\gamma=0.9$ in (97) unless otherwise noted. We note that the present meanings of *rtol* and *atol* as used by *NDSolve* and the *G-Scheme* are somewhat different.

### 5.1. A planar ODE model

As a test featuring stiff explosive/dissipative nonlinear behavior, we use the Semenov model, which represents the dynamics of the first-order exothermal batch reaction $A\rightarrow B$ in a well-stirred jacketed reactor:

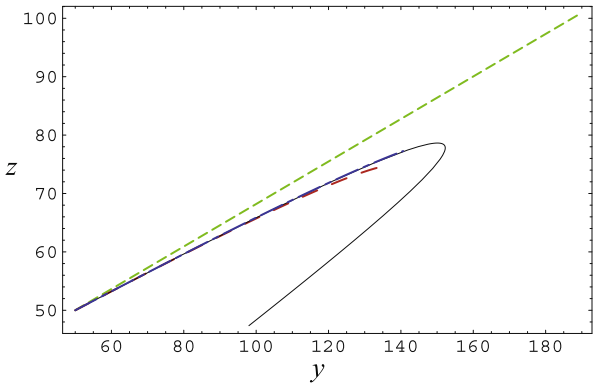


**Fig. 3.** Trajectories obtained for $\tau \in [0, 5\tau_2 = 5\epsilon], \psi = \pi/7, \theta = \pi/9, \epsilon = 0.1$, and initial condition $\{z_0 = 50, y_0 = 50\}$: fast reduced models (128) and (132) (dash red and short-long-dash blue lines), fast dynamics (without slow correction) (125) (short-dash green line), and exact solution of (108) (solid black line). (For interpretation of the references to color in this figure legend, the reader is referred to the web version of this article.)

$$\frac{dy}{dt} = \varepsilon^{-1} f(y,z) \quad \text{and} \quad \frac{dz}{dt} = g(y,z), \tag{134}$$

where

$$f(y,z) = g(y,z) - \delta y \quad \text{and} \quad g(y,z) = z\exp(y/(1+\beta y)) \tag{135}$$

with parameter values $\beta = 0.21, \delta = 1.0$, and $\varepsilon = 10^{-3}$, and initial condition $\{y(0), z(0)\} = \{5, 2\}$. The bifurcation properties of this model have been studied in [29]. This model problem is aimed at illustrating the operating characteristics of the *G-Scheme*.

For this set of parameters the solution proceeds from the initial condition to a fixed point (equilibrium), but with a dynamics which is fairly complex, as can be seen from the phase trajectory shown in Fig. 4, or from the time evolution of $y$ shown in Fig. 5. In all figures regarding this model problem, unless noted otherwise, the illustrations on the left are obtained with the time step safety parameter of $\gamma = 0.1$, while that on the right with $\gamma = 0.5$, and the $log_{10}$ scale is used. Clearly the use of larger $\gamma$ leads to a solution obtained with a much smaller number of time steps at the cost of a somewhat larger error. The relative errors for the two cases are shown in Fig. 6. It is clear from the figure that the error increases as $\gamma$ increases. In Figs. 7 and 8 we show the corresponding number of active modes and the values of the head $(H)$ and tail $(T)$ indices. It is clear from Fig. 7 that most of the time it is only necessary to integrate one ODE; integration of both ODEs is only necessary the first time step, and near the sharp corners shown in Fig. 4. From Fig. 8 we also see that from right after the initial condition until after the first turn $H = T = 2$. This indicates that the dynamics is effectively one-dimensional and is controlled by the fast time scale. Afterwards, with the exception of the period spent in negotiating the second turn, the dynamics is again effectively one-dimensional, but this time it is controlled by the slow time scale since $H = T = 1$. All this can be directly confirmed by examining Fig. 9 where the size of the time step is shown as a function of time in the two cases. The total number of time steps necessary to obtain the solutions with $\gamma = 0.1$ and 0.5 are 318 and 63, respectively.

To illustrate the internal mechanics of the *G-Scheme*, Fig. 10 shows the phase trajectory obtained by the reduced model with $\gamma = 0.5$, and with and without making slow (head) and fast (tail) corrections. Note that in this two-dimensional Semenov model, as long as we have one active mode, then at any time only a head or tail correction to active dynamics can be

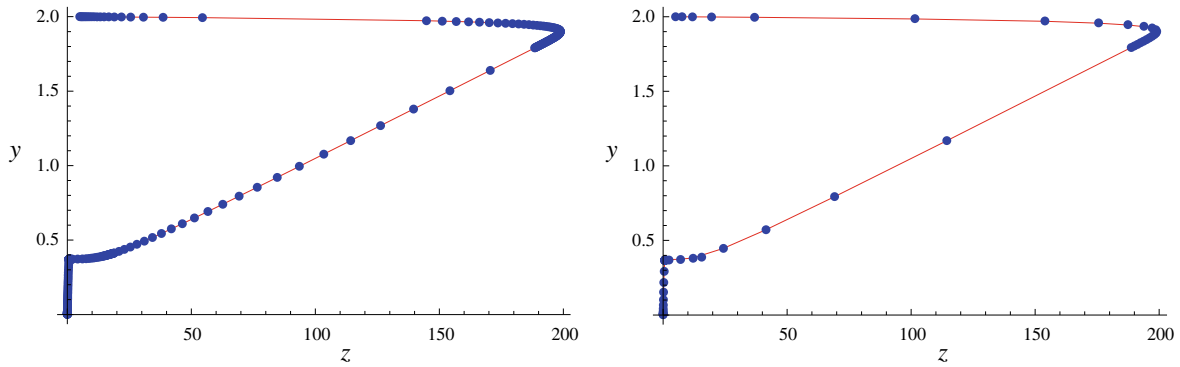


**Fig. 4.** Reference (line) and computed (points) trajectories in the $(y,z)$-plane: (left) $\gamma = 0.1$, (right) $\gamma = 0.5$.

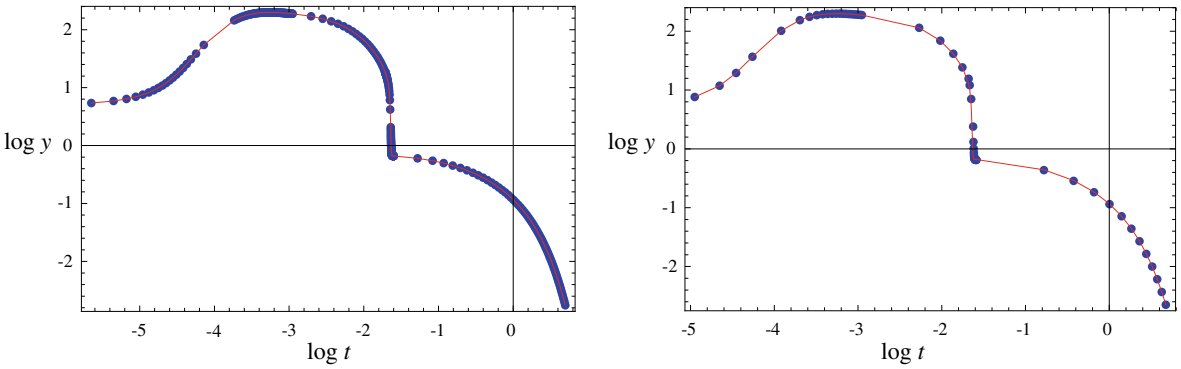


**Fig. 5.** Reference (line) and computed (points) evolution of $y$: (left) $\gamma = 0.1$, (right) $\gamma = 0.5$.

applied. Figs. 11 and 12 show greatly enlarged views of the trajectory near the turning points. We see from Fig. 11 that in the first turn only head corrections are necessary. However, from Fig. 12 we see that small head corrections are applied before the second turn, while tail corrections are necessary after the turn. In Figs. 11 and 12, the blue arrows identify the state vector change due to the active time scales, the red/green arrows are parallel to the slow/fast direction and identify the state vector change due to the application of the head/tail correction, whereas the black arrows refer to the reference solution evaluated at the same time instants as the *G-Scheme* solution. The distance between the points of the red and black arrows or the green and black arrows is the error associated with the particular values of $\gamma$ and *rtol* used in this calculation. A comparison of the plots on the left and right sides of Fig. 11 demonstrates that the addition of the head correction allows to accurately follow the turning of the trajectory in the region where slow scales make important contributions to the dynamics. Comparing the plots on the left and right side of Fig. 12 demonstrates that the addition of the tail correction allows to project

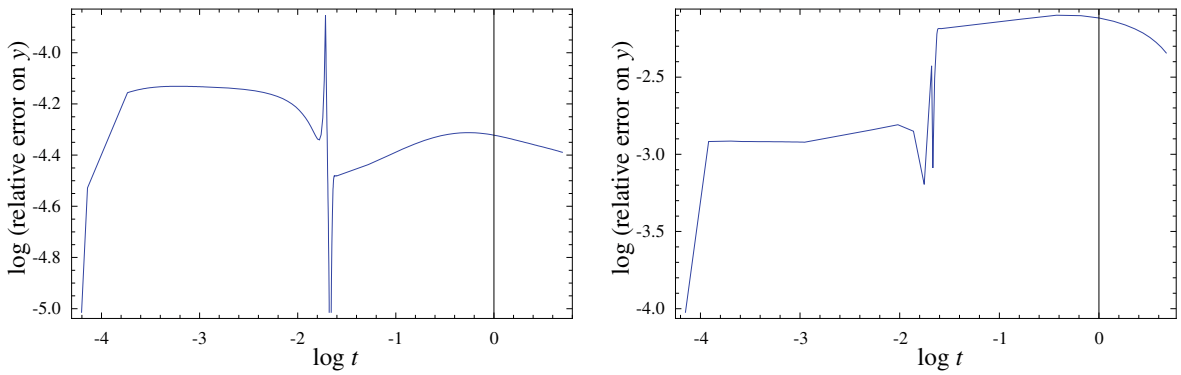


**Fig. 6.** Relative error on $y$: (left) $\gamma = 0.1$, (right) $\gamma = 0.5$.

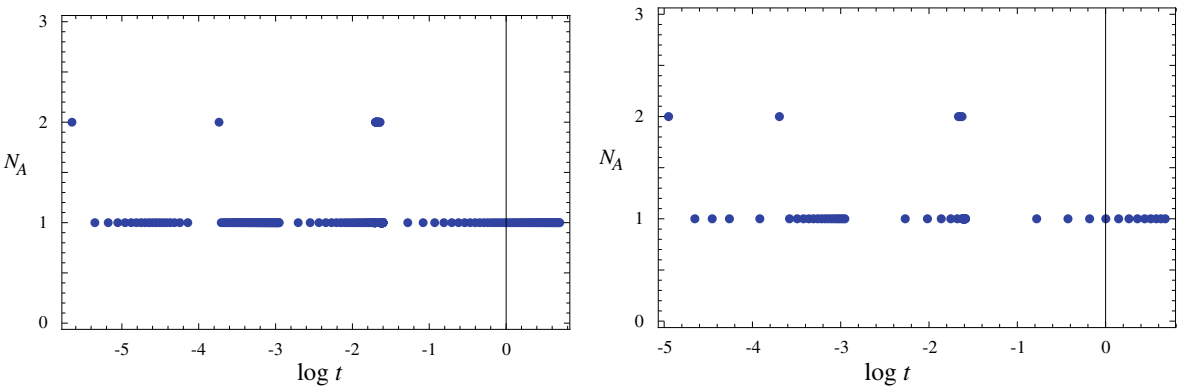


**Fig. 7.** Number of active modes $N_A$ as a function of time: (left) $\gamma = 0.1$, (right) $\gamma = 0.5$.

onto the SIM the state point obtained by the active ODE. Without tail correction, the *G-Scheme* will detect that fast time scales are non-exhausted at the tip of the blue arrow, and will force the integration to proceed with a very small time step (Fig. 15) until the SIM is reached.

We note, by examining Fig. 13, that while the history of the number of active modes remains essentially the same with and without correction, the error and the computational cost become larger. That a reasonable solution is still obtained without corrections, testifies to the robustness of the algorithm. A comparison of the errors is shown in Fig. 14, while from Figs. 11, 12 and 15 we see that the "corrections" in the uncorrected solution is replaced by the integration of the fast dynamics a number of times after each integration of the slow dynamics.

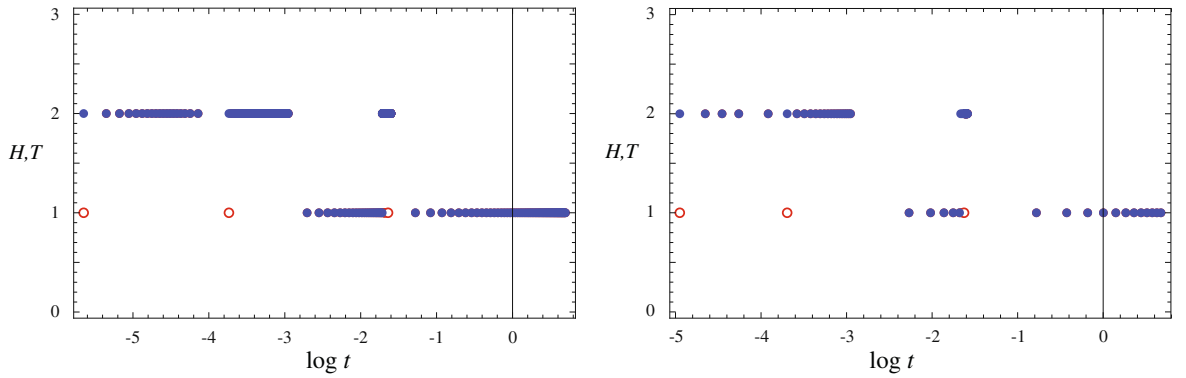


**Fig. 8.** Head $H$ (hollow red circles) and tail $T$ (solid blue circles) indices: (left) $\gamma = 0.1$, (right) $\gamma = 0.5$. (For interpretation of the references to color in this figure legend, the reader is referred to the web version of this article.)

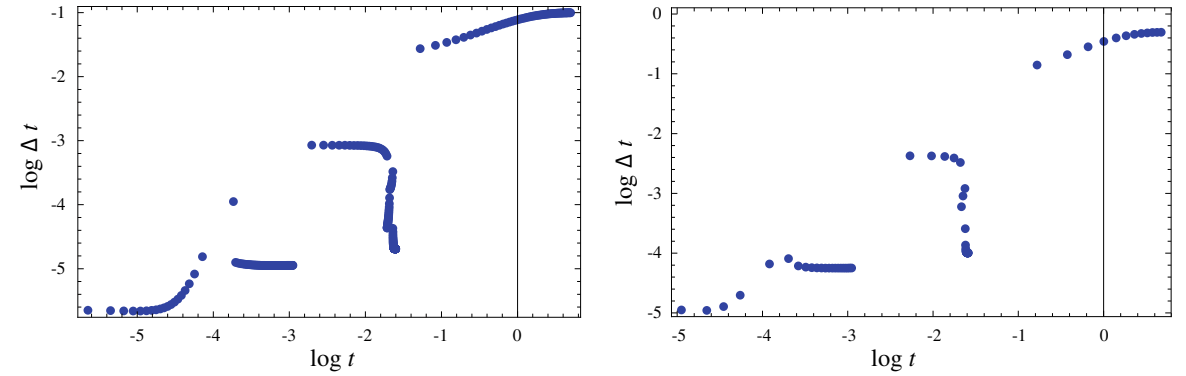


**Fig. 9.** Time step $\Delta t$ as a function of time: (left) $\gamma = 0.1$, (right) $\gamma = 0.5$.

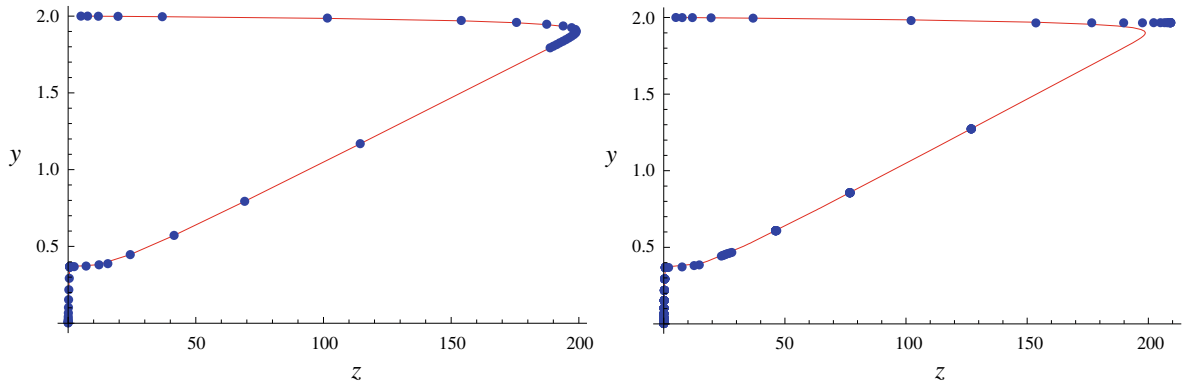


**Fig. 10.** Reference (line) and computed (points) trajectories in the $(y,z)$-plane for $\gamma = 0.5$: with (left) and without (right) head and tail corrections.

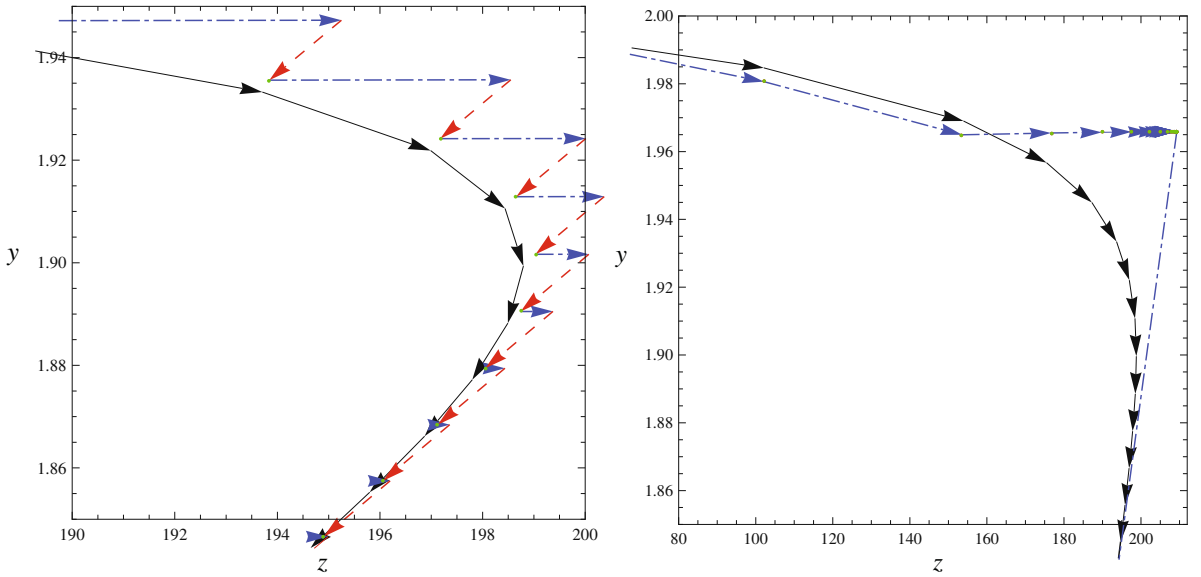


**Fig. 11.** Variations of state vector in the $(y,z)$-plane for $\gamma = 0.5$: reference (black line), active scales (short-long-dash blue line), head correction (long-dash red line), tail correction (short-dash green line): (left) with corrections, (right) without corrections. (For interpretation of the references to color in this figure legend, the reader is referred to the web version of this article.)

### 5.2. A multi-dimensional ODE model

As a test model featuring a complicated nonlinear behavior we consider the isobaric CSTR at very low pressure involving $CO/H_2$ kinetics proposed by Brad et al. [30]. The kinetic mechanism involves 11 species and 33 reactions. The set of ODEs involves 11 rate equations and the energy conservation equation for the molar concentrations and temperature representing the state of the CSTR:

$$\dot{C}_i = \omega_i + \frac{(C_i^0 - C_i)}{t_R}, \quad C_i(0) = C_i^0, \quad \text{for } i = 1,\ldots,11, \tag{136}$$

$$c_p C_{tot} \dot{T} = \sum_i \left( C_i^0 \frac{(H_i^0 - H_i)}{t_R} - \omega_i H_i \right) + U(T_A - T), \quad T(0) = T^0, \tag{137}$$

where $C_i = (p^0/(RT^0))X_i$ is the molar concentration of species $i$, $p^0$ is the constant inlet and reactor pressure, $X_i$ is the mole fraction, $T$ is the reactor temperature, $T_A$ is the constant temperature of the surrounding, $t_R = 8$ s is the residence time, $C_{tot}$ is the total molar concentration, $c_p$ is the specific heat at constant pressure of the mixture, $H_i$ is the molar enthalpy of the $i$-th species, $U = 1600\ \mathrm{J/(K\ m^3\ s)}$ is a heat transfer parameter, $\omega_i$ is the rate of production of the $i$th species, and the zero superscripts denote properties evaluated at the inlet conditions. The inlet molar fraction composition is $\{X^0_{H_2}, X^0_{O_2}, X^0_{CO}\} = \{0.005, 0.5, 0.495\}$ for all test conditions, and we take the inlet temperature to be the same as the exterior temperature, i.e., $T^0 = T_A$. The constants in this system, as well as all other constitutive relations, are the same as in [30].

The CSTR is an open system which possesses three invariants, one for each atomic species, with characteristic time scales equal to $t_R$. These time scales originate from the linear terms in $C_i$ in the balance Eq. (136). This has the effect of shifting the invariant eigenvalues from 0 to $-1$; this change is easily handled within the algorithm. We expect that the *G-Scheme* is able to identify the invariant subspace $\mathbb{C}$, and compute the contributions to the perturbations of the state variables within the range $N_E + 1 = 3 + 1 = 4$ to $N_T$; i.e., it will force the state variable perturbations to lie in the subspace $\mathbb{NC} - \mathbb{T}$.

The dynamics of this system features different types of asymptotic behavior (fixed point, limit cycle, and chaotic attractor). We will present results relative to three values of $\{p^0, T^0\}$ chosen on the basis of the bifurcation diagram produced in [31], each corresponding to one of the three different qualitative asymptotic behaviors.

#### 5.2.1. Fixed point

The inlet condition for this case is $\{p^0, T^0\} = \{14\ \mathrm{Torr}, 735\ \mathrm{K}\}$. The time evolution of the temperature is shown in Fig. 16, from which it is apparent that after $t > 10^{-1}$ the temperature levels off to its stationary value. The figure also shows the relative error between the temperature evolution computed by the *G-Scheme* and the reference computed by *ND-Solve*: the error is always below 0.1%, this maximum value being reached during the explosive stage, whereas the error drops by several orders of magnitude during the relaxation towards the fixed point. It is expected that during the period of large temperature changes, the number of active time scales is large leading to a large number of active ODEs to be solved, whereas at large

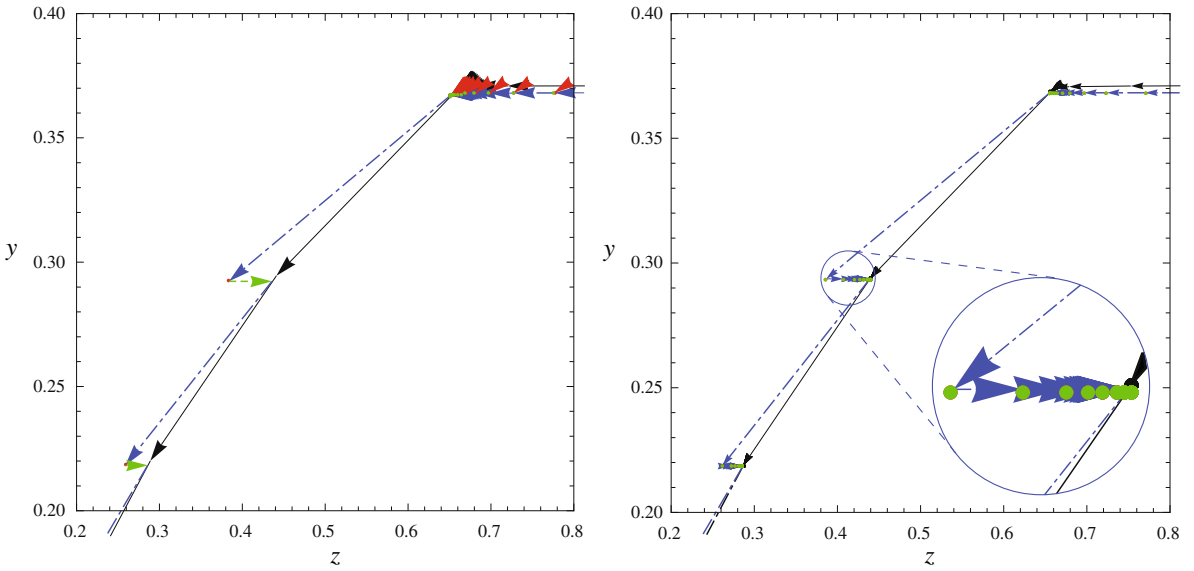


**Fig. 12.** Variations of state vector in the $(y,z)$-plane with $\gamma = 0.5$: reference (black line), active scales (short-long-dash blue line), head correction (long-dash red line), tail correction (short-dash green line): (left) with corrections, (right) without corrections. (For interpretation of the references to color in this figure legend, the reader is referred to the web version of this article.)

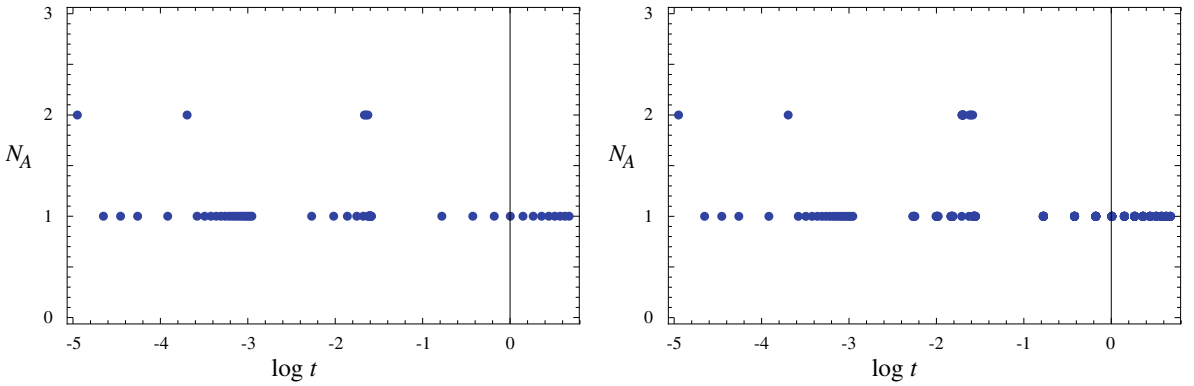


**Fig. 13.** Number of active modes $N_A$ as a function of time for $\gamma = 0.5$: (left) with corrections, (right) without corrections.

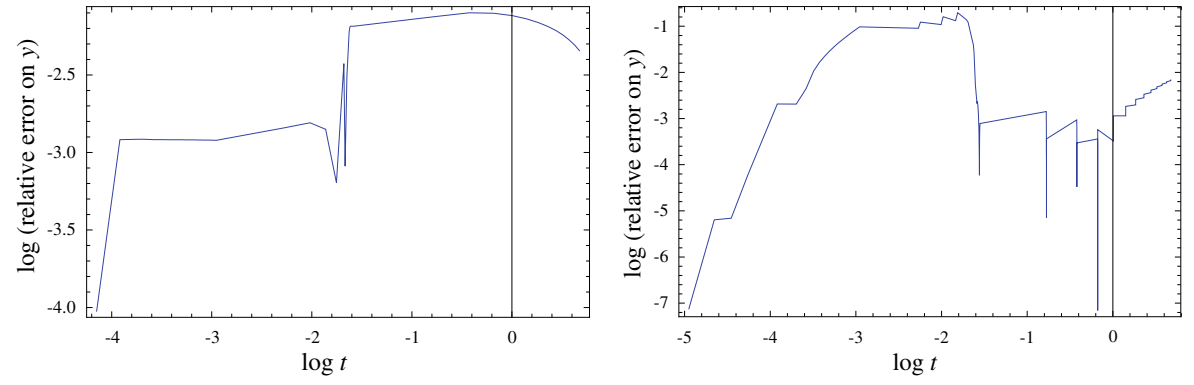


**Fig. 14.** Relative error on $y$ for $\gamma = 0.5$: (left) with corrections, (right) without corrections.

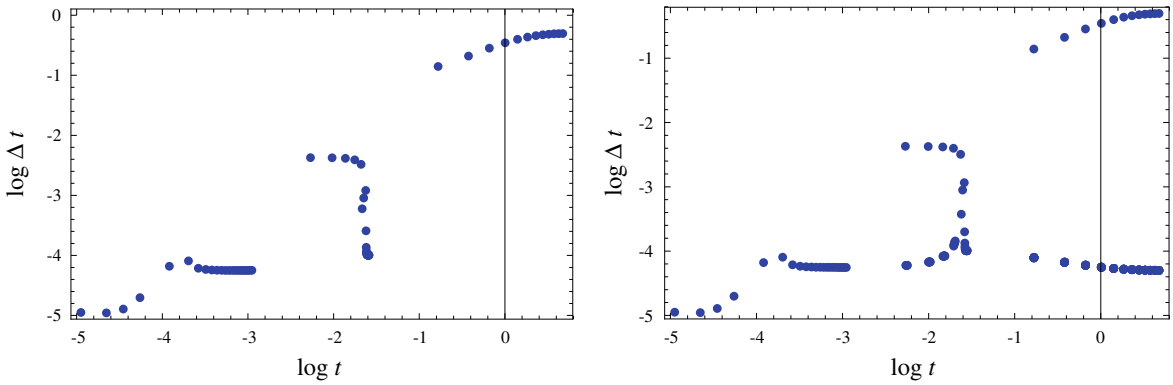


**Fig. 15.** Time step $\Delta t$ as a function of time for $\gamma = 0.5$: (left) with corrections, (right) without corrections.

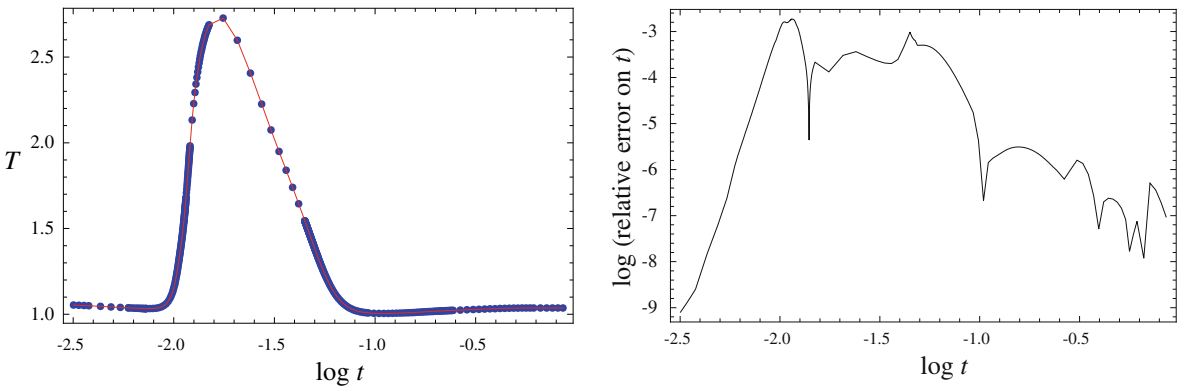


**Fig. 16.** (left) Evolution of $T$: reference (line) and computed (points) solutions, and (right) relative error on $T$.

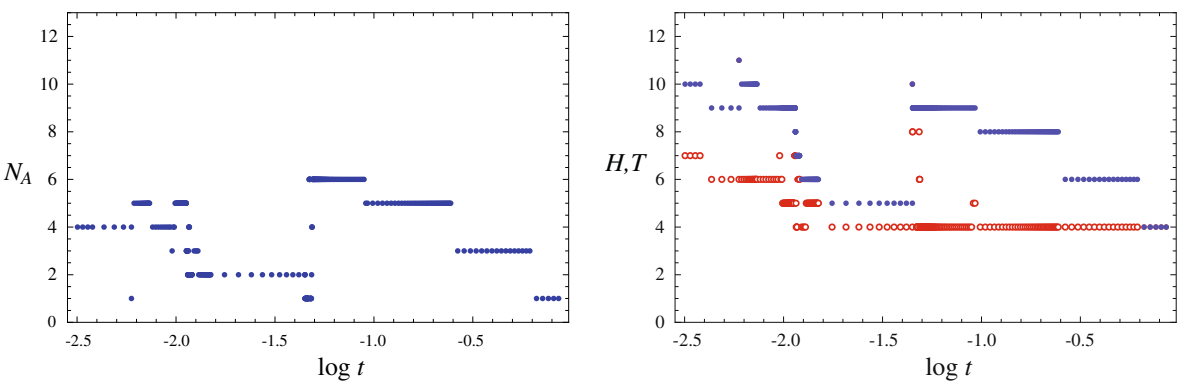


**Fig. 17.** (left) Number of active modes $N_A$, and (right) values of head $H$ (hollow red circles), and tail $T$ (solid blue circles), indices. (For interpretation of the references to color in this figure legend, the reader is referred to the web version of this article.)

times, under near-equilibrium condition, we expect many exhausted fast time scales and a corresponding, progressive reduction of active ODEs. The large temperature changes are accompanied by a large rate of change of the Jacobian matrix, which denotes significant nonlinear effects and large rotations of the basis vectors. These expectations are indeed confirmed by examining Fig. 17, which shows, more specifically, that the approach to the fixed point proceeds with only one ODE with a time scale corresponding to a very large integration time step. Also note in Fig. 17, that the relaxation towards the equilibrium starts at time $t \approx 10^{-1.3}$, where $N_A = 6$; as time advances, $N_A$ takes the values 5, 3, and finally 1. Each $N_A$ corresponds to a SIM of equivalent dimension, this indicating that the (slow) approach to equilibrium occurs through a succession of embedded SIMs.

the last subspace increases (I decreases
the stiffness in the problem, thus allowing the sl
tering any numerical instability. In Fig. 18(right),
system. The strip comprised of time scales betw
active subspace evolution, its narrowing indicat
problem and exploited computationally by the
to the development of SIMs of different dimen
with respect to the active ones.

### 2.2. Limit cycle

To test the *G-Scheme* under more sever
$T^0\} = \{14$ Torr,680 K$\}$. The temperature
ugh we do not present additional deta
and $HO_2$ peak, followed by a relaxa
which $HO_2$ is produced, with the l
rror in $T$ is below 1%, this max
lers of magnitude during th
n Fig. 19, Fig. 20 demon
as witnessed by th
mbedding dim

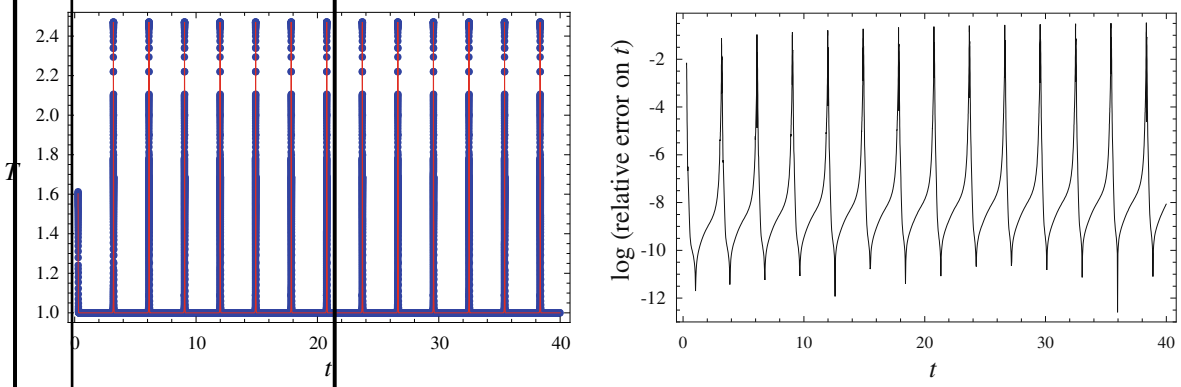


**Fig. 19.** Evolutions of (left) $T$ from *NDSolve* (red line) and *G-Scheme* (blue points), and (right) relative error on $T$. (For interpretation of the references to color in this figure legend, the reader is referred to the web version of this article.)

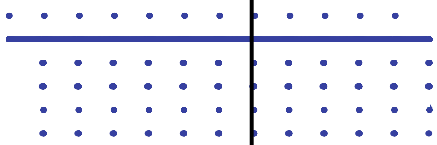

choices of head and tail time scales made by the *G-Scheme*. Figs. 20(right) and 21(right) show that during the explosive regime both $T$ and $H$ increase in such a way that their difference decreases. Thus, although the driving time scale $\tau_T$ becomes small during the explosions because of the larger value of $T$, the degree of reduction increases, ($N_A$ attains unit value). Instead, in-between two successive explosions, $H$ and $T$ attain constant values (4 and 8, respectively), so that $N_A$ remains uniformly equal to 5. The analysis of the evolution of the time rate of change of $J$ demonstrates that the system has a nearly linear behavior (also confirmed in Fig. 21(right) by the small changes of the time scales), whereas the nonlinearities are confined within the explosions.

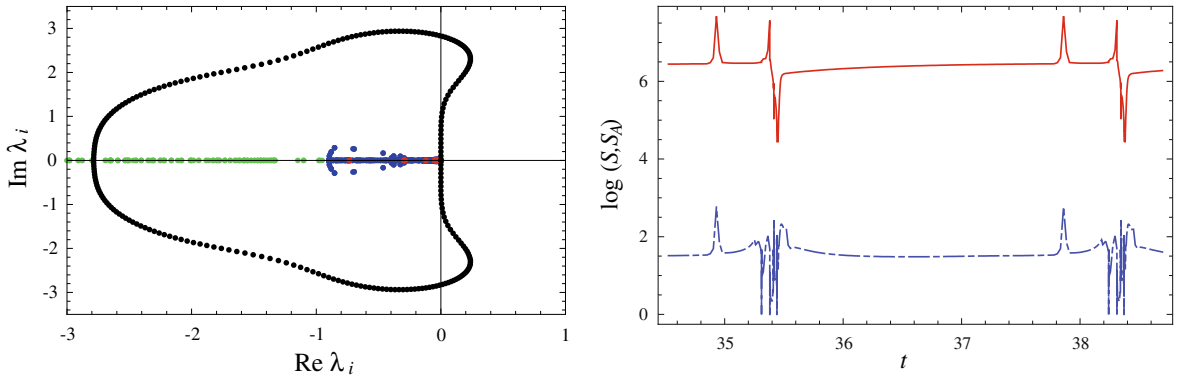


**Fig. 22.** (left) Detail of the spectra and stability boundary of RK4: stability boundary (black points), active eigenvalues (blue), slow eigenvalues (red), and fast eigenvalues (green). (right) Stiffness parameters of the complete system $S$ (red line), and of the active dynamics $S_A$ (short-long-dash blue line), during one cycle orbit. (For interpretation of the references to color in this figure legend, the reader is referred to the web version of this article.)

In Fig. 22(left) we also display an enlarged region of the union of the spectra over the complete time history. It is noted that the eigenvalues corresponding to active modes are all comfortably within the stability region of the ERK4 scheme. Furthermore, all modes corresponding to eigenvalues having nearly zero magnitude while always comfortably within the stability region, are nevertheless also effectively accounted for through the head correction. It should also be noted that the problem is very stiff, but the stiffness is removed since all modes corresponding to the eigenvalues having large magnitude are effectively accounted for through the tail correction. The stiffness reduction ratio $S/S_A$ resulting from the use of the *G-Scheme* is approximately $10^5$ during a complete cycle orbit (Fig. 22(right)). The combination of "reducing" the largest and "increasing" the smallest eigenvalues present in the dynamics reduces substantially the stiffness in the problem. Nevertheless, the accuracy is retained by accounting for both the fast and slow modes through head and tail corrections.

The degree of accuracy of the applied corrections can be estimated by examining Fig. 23. With the exception of the period during the explosive phase, the tail spectral gap remains sufficiently small (near $10^{-0.7} \approx 0.2$), while the spectral separation between the driving mode and the fastest of the slow modes is much smaller (near $10^{-1.5} \approx 0.03$) during most of the orbit, but is always less than $10^{-0.5} \approx 0.3$ during the complete cycle.

*5.2.3. Chaotic attractor*

Prescribing the initial condition $\{p^0, T^0\} = \{21.8\ \text{Torr}, 735\ \text{K}\}$ yields the chaotic behavior portrayed in the ($H_2O$, O) phase portrait shown in Fig. 24, while the corresponding time histories of CO and its relative error over a limited time interval are reported in Fig. 25. The results obtained here are with $\gamma = 0.75$. We note that the error in the trajectory is between $10^{-4}$ and $10^{-1}$. Inspection of Fig. 26 shows that the number of active ODEs oscillates about a value of 4, obtained using a constant head index of $H = 4$, resulting from the dimension of the invariant subspace, and a tail index varying between $T = 6$ and 8. Thus, the approximate dimension of the asymptotic dynamics of the CSTR model problem is 8, whereas the average number of active equations weighed with respect to time, is near 4. The time histories of the size of the time step and of the time scales is shown in Fig. 27. Also on the figure are indicated the variations of the slow and fast time scales as identified by the *G-Scheme*. Differently from the case of the limit cycle dynamics, we note in Fig. 27(right) that significant nonlinearities occur at all times in the fast subspace.

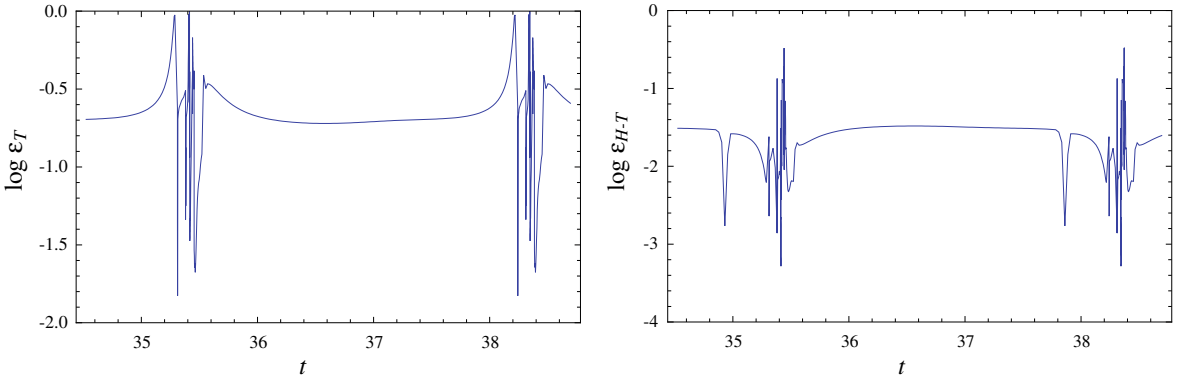


**Fig. 23.** (left) Tail spectral gap $\epsilon_T$, and (right) spectral distance $\epsilon_{H-T}$, during one cycle orbit.

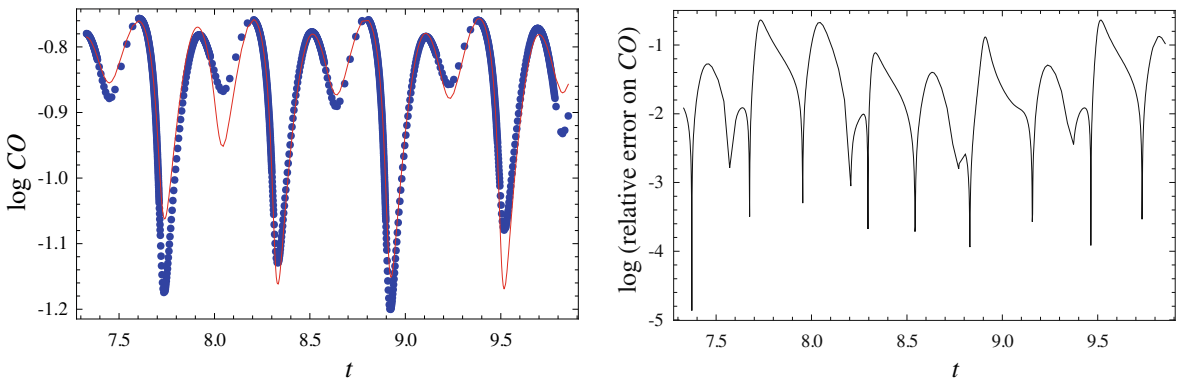


**Fig. 25.** Evolutions of (left) CO from

It is apparent that while the evolutions are chaotic, the average size of the time step is approximately $10^{-3}$ and the active modes have time scales approximately between $10^{-3}$ and $10^{-0.2}$. In Fig. 28(left) we show an enlarged region of the union of the spectra over the complete time history. As in the periodic attractor case, it is noted that the eigenvalues corresponding to

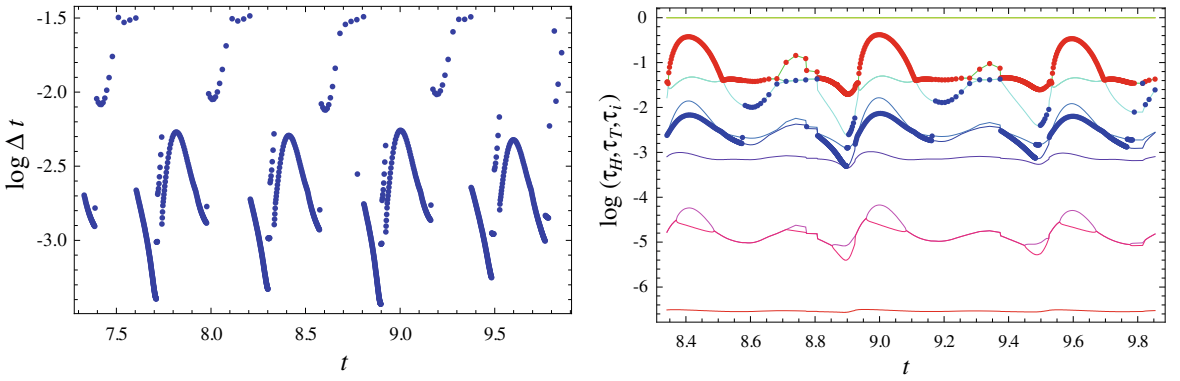


**Fig. 27.** Evolutions of (left) time step, and (right) head time scale (red points), tail time scale (blue points), and all other time scales (lines). (For interpretation of the references to color in this figure legend, the reader is referred to the web version of this article.)

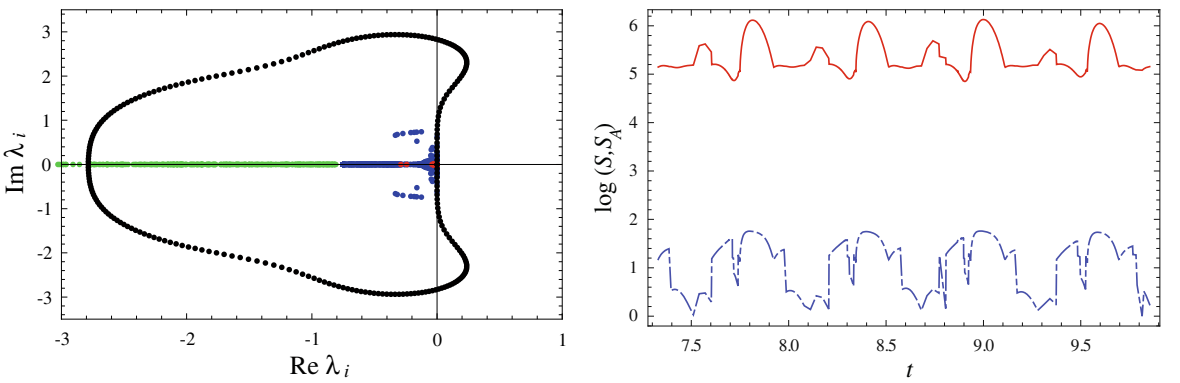


**Fig. 28.** (left) Detail of the spectra and stability boundary of RK4: stability boundary (black points), active eigenvalues (blue), slow eigenvalues (red), and fast eigenvalues (green); (right) stiffness parameters of the complete system $S$ (red line), and of the active dynamics $S_A$ (short-long-dash blue line). (For interpretation of the references to color in this figure legend, the reader is referred to the web version of this article.)

active modes are all comfortably within the stability region of the ERK4 scheme, and that the stiffness of the system is substantially reduced by accounting for the slow and fast modes using asymptotic corrections. It can be seen that the stiffness reduction ratio $S/S_A$ resulting from the use of the *G-Scheme* is approximately $10^5$ (Fig. 28(right)). The degree of accuracy of the corrections applied by the scheme can be estimated by examining the tail spectral gap $\epsilon_T$ and the spectral separation between the fastest of the slow modes and the driving mode $\epsilon_{H-T}$ shown in Fig. 29. We see that on the average $\epsilon_T \approx 10^{-0.5} \approx 0.3$ and $\epsilon_{H-T} \approx 10^{-1}$. Clearly, during the periods of time in which these values are larger, the accuracies of the corrections are lower, while when these values are smaller, the corrections are more accurate. Fig. 27(right) shows that

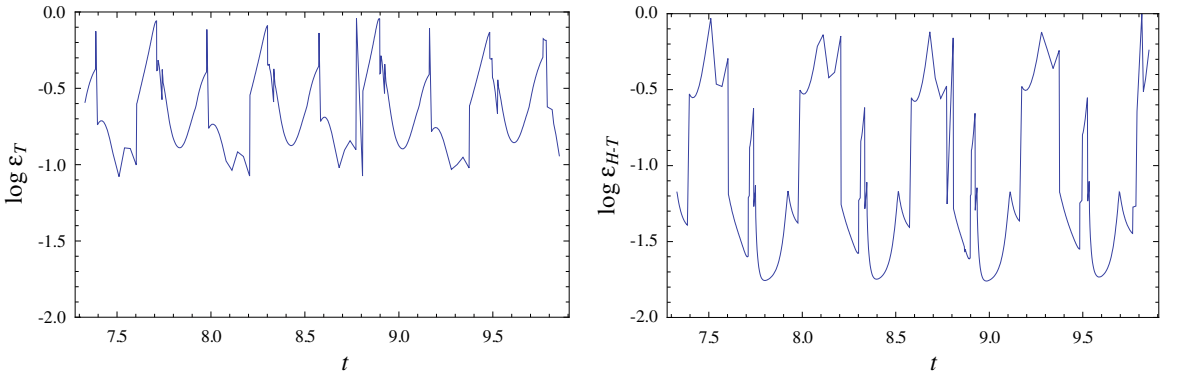


**Fig. 29.** (left) Tail spectral gap $\epsilon_T$, and (right) spectral distance $\epsilon_{H-T}$, during one cycle orbit.

along the chaotic attractor we have eigenvalues with large imaginary components, indicating that this dynamics is not well suited to the *G-Scheme*, which has been designed for systems with eigenvalues having dominant negative real parts.

### 5.3. A PDE model

As a typical reaction–diffusion model exhibiting a rich dynamic structure, we consider the model proposed by Elezgaray and Arneodo [28], henceforth referred to as the EA model for short. The EA model is a system of two coupled nonlinear PDEs:

$$\begin{aligned}\frac{\partial u}{\partial t} &= D\frac{\partial^2 u}{\partial x^2} + \epsilon^{-1}(v - (u^2 + u^3)),\\ \frac{\partial v}{\partial t} &= D\frac{\partial^2 v}{\partial x^2} - u + \alpha\end{aligned} \tag{138}$$

in $(u(x,t), v(x,t)), (x,t) \in ([0,1],[0,\infty))$, representing the concentrations of two chemical species with an isothermal explosive kinetics displaying intermittent bursting for some values of the parameters. Here, $D, \alpha$, and $\epsilon$ are positive parameters. The system (138) is solved with boundary conditions $u(0,t) = u(1,t) = -2$ and $v(0,t) = v(1,t) = -4$ for $t > 0$, and initial conditions $u(x,0) = v(x,0) = 0$ for $x \in [0,1]$.

For small and large values of diffusion $D$, the system stabilizes onto ignited and extinguished steady states, respectively. Intermediate values of $D$ correspond to operating conditions that allow competition between the tendency to ignition due to the nonlinear kinetics, and the extinguishing behavior at the boundaries. This induces complex oscillations and intermittent bursting in the center of the spatial domain. In this case, no invariants are present, hence $E = 0$.

The discrete form of the set of PDEs is obtained by using a second-order three-points finite difference approximation of the Laplacian operator, and subsequently solved using the method of lines using *NDSolve* for the reference solution and ERK4 for the *G-Scheme* solution. The calculations are obtained by setting $D = 0.032, \alpha = 0.01$ and $\epsilon = 0.01$ so as to obtain a limit cycle behavior. We use $N = 32, 64$ and 128 spatial cells. Iso-contours of $u(x,t)$ and $v(x,t)$ corresponding to the reference solution is given in Fig. 30. Note that all tests we perform below use the same number of spatial cells in the reference solution as well as in the solution obtained by the *G-Scheme*; the two solutions differ only in the treatment of time integration. The evolutions of $u(x,t)$ and $v(x,t)$ at the mid-point $x = 0.5$ are displayed in Fig. 31. The relative errors on $u$ and $v$ at the mid-point as functions of time are shown in Fig. 32; we see that the error on $u$ is typically less than $10^{-2}$ except during the fast bursting periods, while that on $v$ is always less than $10^{-2}$. Note that these are just errors due to the approximate temporal treatment of the *G-Scheme*. The error due to the spatial discretization is not relevant to the present discussion.

In Fig. 33 we show the evolution of the number of active equations $N_A$. After the initial transient during which the system approaches the limit cycle, $N_A$ attains a periodic behavior where the minimum value is 7 and the maximum is approximately 50. In Fig. 34 we plot the number of active modes $N_A$ for $N = 32, 64$, and 128 as functions of time. From the figure we clearly see that $N_A$ becomes essentially independent of the spatial resolution! This fact can be understood by considering that the number of positive Lyapunov exponents in this problem is 5; thus, the embedding dimension of the asymptotic dynamics of the problem is 7 when the central manifold, corresponding to the zero exponent, is included together with at least one stable mode [22]. If we evaluate the average number of active equations weighed with respect to time for a number of cells equal to 32, 64, and 128, we obtain 15.12, 13.24, and 14.22, respectively, whereas the minimum number of active equations is 7, which is the same as the embedding dimension.

An important consequence of this finding is that the number of active ODEs generated by the *G-Scheme* in this case is suboptimal in the sense that it is somewhat larger than the minimum number of degrees of freedom required to describe the

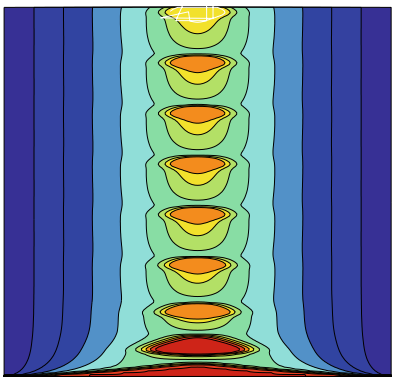

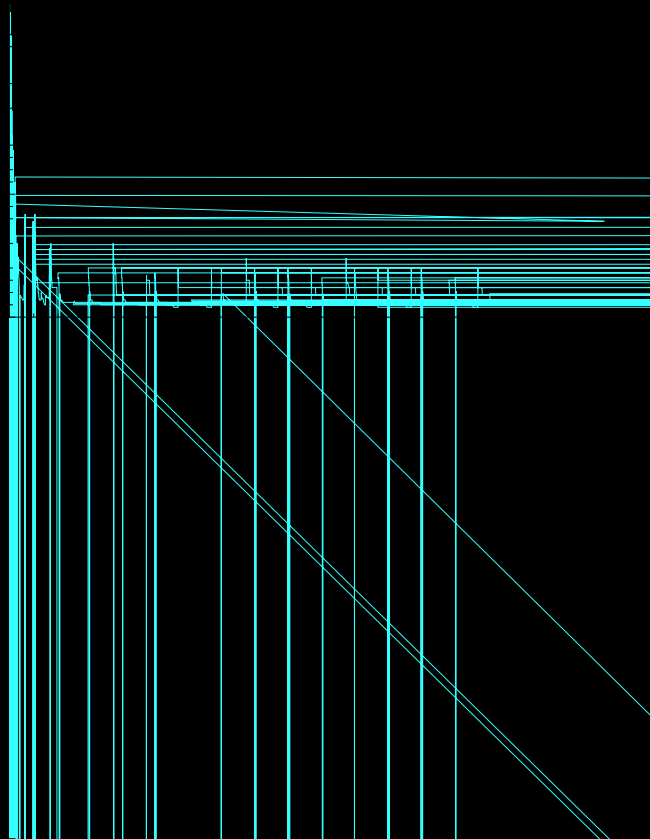

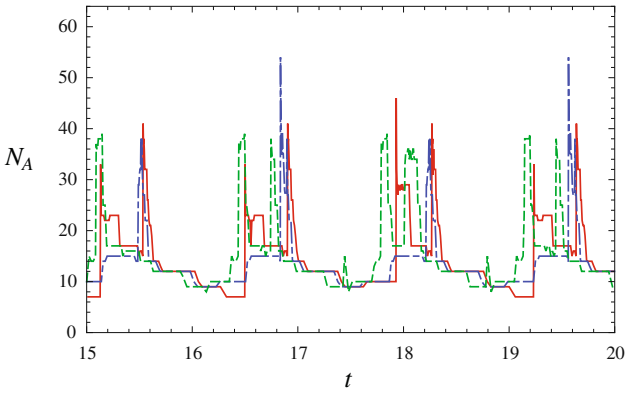


**Fig. 34.** Evolutions of $N_A$ for $n = 32$ (short-dash green line), $n = 64$ (short-long-dash blue line), and $N = 128$ (red line). (For interpretation of the references to color in this figure legend, the reader is referred to the web version of this article.)

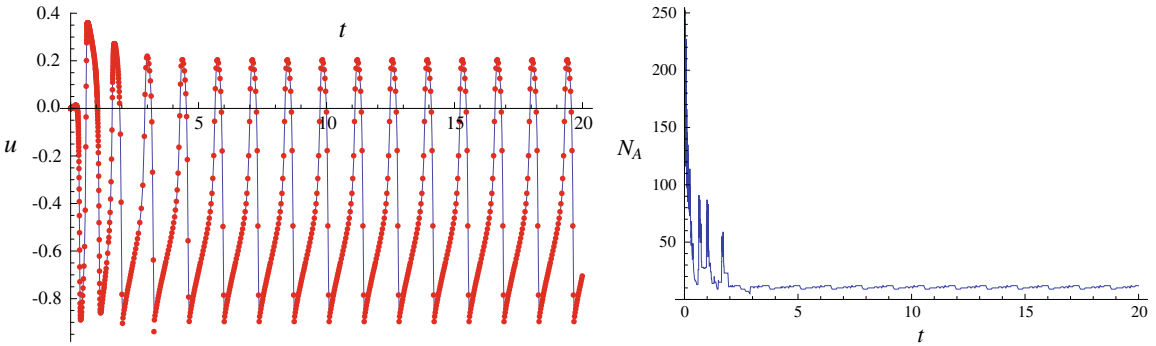


**Fig. 35.** Evolutions of (left) $u$ at $x = 0.5$, *ND-Solve* (line) and *G-Scheme* (points); (right) $N_A$, for $N = 128$ and $T_{\max} = 12$.

Lastly, as pointed out in Remark 9, $N_T$ might be prescribed by specifying that time scales smaller than a threshold $\tau_{\min}$ should not be considered within the active ODE set; i.e., that $T$ not be larger than a prescribed index value $T_{\max}$. In testing this idea, we find that the smallest $T_{\max}$ that yields a sufficiently accurate solution of the EA problem is 12, as demonstrated by the results reported in Fig. 35 which can be compared with those in Figs. 31(left) and 33(left) referring to the calculations with adaptive $T$. From these results we see that a static model valid along the limit cycle can be built with at most 12 modes given that $T_{\max} = 12$ for times larger than the initial transient period.

In Fig. 36 we compare the time step evolutions obtained with $N = 128$ with adaptive $T$ and $T_{\max} = 12$. The figure shows that in the latter case the time step undergoes small amplitude variations about an average of approximately $10^{-1.6} \approx 2.5 \times 10^{-2}$, whereas in the first case the enforced tolerance of $rtol = 10^{-4}$ forces $\Delta t$ to attain the value of

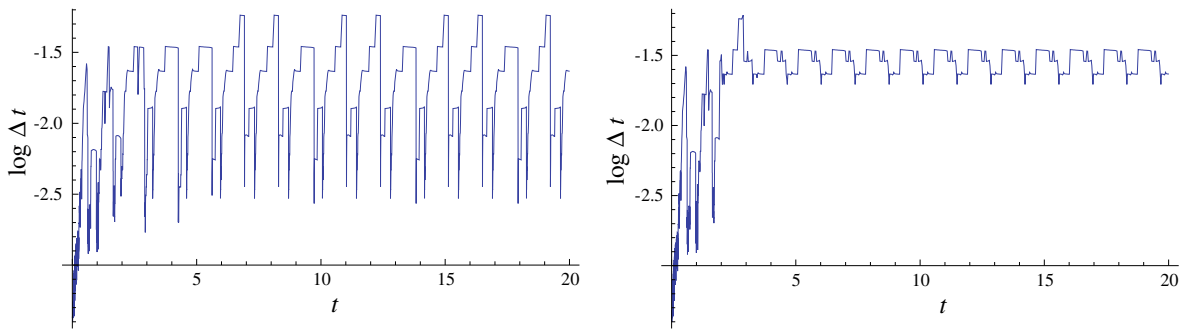


**Fig. 36.** Evolutions of time step for $N = 128$ with (left) adaptive $T$ and (right) $T_{\max} = 12$.

Clearly, the *G-Scheme* will be as efficient as, say, an implicit BDF scheme when the total work reduction will more than balance the costs associated with the spectral characterization of the problem. Optimization of the *G-Scheme* and a careful cost analysis will be the subject of a forthcoming investigation. Among possible improvements of the computational efficiency of the scheme one could resort to the exploitation of the knowledge at previous time steps to obtain useful information at the current time level.

Another important aspect that will also be the subject of future work is a careful error analysis to provide an estimate of the overall accuracy of the algorithm, or more importantly to provide a solution with a given (precise) accuracy. There are multiple sources of inaccuracy in the *G-Scheme*:

- Inaccuracy in the solution of the active DEs, especially with regard to the approximation of neglecting the rotation of the basis vectors which define the local change of frame of reference. This error can be controlled by either reducing the size of the time step, when the time rate of change of the rotation of the basis vectors is large (i.e., when nonlinearities are important), so that the terms in the equations that involve the rotation of the basis vectors are of higher order, or by including such terms in an explicit fashion.
- Inaccuracy of the explicit numerical method used to solve the active DEs. This error can be reduced/controlled by the use of an inner variable time integration step to ensure a prescribed accuracy for the solution, and/or using a variable order time integration scheme.

- Inaccuracy due to the slow/fast decoupling, that is quality of the basis vectors, which affects both the efficiency of the scheme by purifying the active DEs from both the slow and fast time scales, and the accuracy of the identification of the SIM. For problems in which $\epsilon_H \ll 1, \epsilon_{H-T} \ll 1$ and $\epsilon_T \ll 1$, these errors are expected to be exponentially small. However, when no clear spectral gaps exist, these errors can be reduced by appropriately increasing the number of active modes so as to satisfy a user-prescribed accuracy level.

Having reviewed what remains to be done, we want to conclude by stressing that the main goal of this paper is the presentation of the *G-Scheme* framework and the verification of its ability in achieving an adaptive model reduction. Regarding this aspect, the validation carried out by considering a range of test cases involving both linear and nonlinear behavior, both ODEs and PDEs, containing both simple and nontrivial asymptotic dynamics, has successfully demonstrated the potential of the *G-Scheme*. We already have successfully tested the *G-Scheme* in problems related to the kinetics of large hydrocarbons (propane, *n*-heptane) involving up to 560 species and 2538 reversible reactions [32], and lastly in problems related to biological systems. Clearly, it is outside the scope of this paper to report about these findings, which will be considered in forthcoming papers. In addition to addressing issues related to computational efficiency and error analysis, much work is still needed to translate this framework into a useful computational tool. We plan to make the package available to users and voluntary developers under the open-source paradigm in the near-future.

## Acknowledgments

MV acknowledges the support of the Italian Ministry of University and Research (MIUR) and the US Department of Energy, Office of Basic Energy Sciences, SciDAC Computational Chemistry Program. SP worked on the *G-Scheme* during his sabbatical stay in the Department of Mechanics and Aeronautics at the University of Rome "La Sapienza" thanks to the support from the University of Notre Dame, NASA (Award #NNX07AD10A), and NSF (Award #0650843).

## References

[1] T. Echekki, J.H. Chen, Unsteady strain rate and curvature effects in turbulent premixed methane–air flames, Combust. Flame 106 (1996) 184–202.
[2] S. Singh, Y. Rastigejev, S. Paolucci, J.M. Powers, Viscous detonation in $H_2 - O_2$–Ar using intrinsic low-dimensional manifolds and wavelet adaptive multilevel representation, Combust. Theory Modell. 5 (2001) 163–184.
[3] L.A. Segel, M. Slemrod, The quasi steady state assumption: a case study in perturbation, SIAM Rev. 31 (1989) 446–447.
[4] A.N. Yannacopoulos, A.S. Tomlin, J. Brindley, J.H. Merkin, M.J. Pilling, The error of the quasi steady state approximation in spatially distributed systems, Chem. Phys. Lett. 248 (1996) 63–70.
[5] D.A. Goussis, On the construction and use of reduced chemical kinetics mechanisms produced on the basis of given algebraic relations, J. Comput. Phys. 128 (1996) 261–273.
[6] A. Massias, D. Diamantis, E. Mastorakos, D.A. Goussis, An algorithm for the construction of global reduced mechanisms with CSP data, Combust. Flame 117 (1999) 685–708.
[7] U. Maas, S.B. Pope, Simplifying chemical kinetics: intrinsic low dimensional manifolds in composition space, Combust. Flame 88 (1992) 239–264.
[8] S.B. Pope, Computationally efficient implementation of combustion chemistry using *in situ* adaptive tabulation, Combust. Theory Modell. 1 (1997) 41–63.
[9] S.R. Tonse, N.W. Moriarty, N.J. Brown, M. Frenklach, PRISM: piecewise reusable implementation of solution mapping. An economical strategy for chemical kinetics, Israel J. Chem. 39 (1999) 97–106.
[10] T. Lu, C.K. Law, Linear time reduction of large kinetic mechanisms with directed relation graph: *n*-heptane and iso-octane, Combust. Flame 30 (2006) 24–36.
[11] P. Pepiot, H. Pitsch, Systematic reduction of large chemical mechanisms, in: Proceedings of the Fourth Joint Meeting of the US Sections of the Combustion Institute, 2005.
[12] M. Valorani, F. Creta, D.A. Goussis, H.N. Najm, J.C. Lee, An automatic procedure for the simplification of chemical kinetics mechanisms based on CSP, Combust. Flame 146 (1–2) (2006) 29–51.
[13] T. Løvås, F. Mauss, C. Hasse, N. Peters, Development of adaptive kinetics for application in combustion systems, Proc. Combust. Inst. 29 (2002) 1403–1410.
[14] P. Pepiot-Desjardins, H. Pitsch, An automatic strategy to develop reduced kinetic mechanisms for surrogate fuels, in: International Workshop on Model Reduction in Reacting Flow, September 3–5, 2007.
[15] V.I. Oseledec, A multiplicative ergodic theorem, Lyapunov characteristic numbers for dynamical systems, Trans. Moscow Math. Soc. 19 (1997).
[16] A. Adrover, F. Creta, M. Giona, M. Valorani, V. Vitacolonna, Natural tangent dynamics with recurrent biorthogonalizations: a geometric computational approach to dynamical systems exhibiting slow manifolds and periodic/chaotic limit sets, Physica D – Nonlinear Phenom. 213 (2) (2006) 121–146.
[17] S.H. Lam, D.A. Goussis, Understanding complex chemical kinetics with computational singular perturbation, Proc. Comb. Inst. 22 (1988) 931–941.
[18] S.H. Lam, Using CSP to understand complex chemical kinetics, Combust. Sci. Technol. 89 (1993) 375–404.
[19] S.H. Lam, D.A. Goussis, The CSP method for simplifying kinetics, Int. J. Chem. Kinet. 26 (1994) 461–486.
[20] N. Fenichel, Geometric singular perturbation theory for ordinary differential equations, J. Differen. Equat. 31 (1979) 53–98.
[21] V. Bykov, I. Goldfarb, V. Gol'dshtein, S. Sazhin, E. Sazhina, System decomposition technique for spray modelling in CFD codes, Comput. Fluids 3 (3) (2007) 601–610.
[22] A. Adrover, F. Creta, M. Giona, M. Valorani, Stretching-based diagnostics and reduction of chemical kinetic models with diffusion, J. Comput. Phys. 225 (2007) 1442–1471.
[23] M. Valorani, D.A. Goussis, Explicit time-scale splitting algorithm for stiff problems: auto-ignition of gaseous-mixtures behind a steady shock, J. Comput. Phys. 168 (1) (2001) 44–79.
[24] J.M. Ortega, H.N. Najm, J. Ray, M. Valorani, D.A. Goussis, M.Y. Frenklach, Adaptive chemistry computations of reacting flow, J. Phys. Conf. Ser. 78 (2007) 012054.
[25] M. Valorani, D.A. Goussis, F. Creta, H.N. Najm, Higher order corrections in the approximation of low dimensional manifolds and the construction of simplified problems with the CSP method, J. Comput. Phys. 209 (2005) 754–786.
[26] A. Zagaris, H.G. Kaper, T.J. Kaper, Analysis of the CSP reduction method for chemical kinetics, Nonlinear Sci. 14 (2004) 59–91.
[27] A. Zagaris, H.G. Kaper, T.J. Kaper, Fast and slow dynamics for the computational singular perturbation method, Multiscale Model. Simul. 2 (2004) 613–638.

[28] J. Elezgaray, A. Arneodo, Crisis-induced intermittent bursting in reaction–diffusion chemical systems, Phys. Rev. Lett. 68 (1992) 714–717.
[29] F. Creta, A. Adrover, S. Cerbelli, M. Valorani, M. Giona, Slow manifold structure in explosive kinetics. 1. Bifurcations of points-at-infinity in prototypical models, J. Phys. Chem. A 110 (50) (2006) 13447–13462.
[30] R.B. Brad, A.S. Tomlin, M. Fairweather, J.F. Griffiths, The application of chemical reduction methods to a combustion system exhibiting complex dynamics, Proc. Combust. Inst. 31 (2007) 455–463.
[31] F. Creta, A. Adrover, M. Giona, M. Valorani, Geometric approaches to model reduction: from invariant to stretching-based subspaces, in: International Workshop on Model Reduction in Reacting Flow, Rome, 2007.
[32] M. Valorani, S. Paolucci, Adaptive model reduction in chemical kinetics, in: R. Ragucci (Ed.), Italian Section of the Combustion Institute, Turin, Italy, 2008.